REPORT DOCUMENTATION PAGE

Form Approved
OMB No. 0704-0188

PLEASE DO NOT RETURN YOUR FORM TO THE ABOVE ORGANIZATION.

1. REPORT DATE *(DD-MM-YYYY)*	2. REPORT TYPE	3. DATES COVERED *(From - To)*
19-06-2013	Journal Article	

4. TITLE AND SUBTITLE

Current and Hydrographic Conditions at the East Flower Garden Bank in 2011

5a. CONTRACT NUMBER

5b. GRANT NUMBER

5c. PROGRAM ELEMENT NUMBER
061153N

6. AUTHOR(S)
W.J. Teague, H.W. Wijesekera, E. Jarosz, D.B. Fribance, A. Lugo-Fernandez and Z.R. Hallock

5d. PROJECT NUMBER

5e. TASK NUMBER

5f. WORK UNIT NUMBER
73-4491-02-5

7. PERFORMING ORGANIZATION NAME(S) AND ADDRESS(ES)
Naval Research Laboratory
Oceanography Division
Stennis Space Center, MS 39529-5004

8. PERFORMING ORGANIZATION REPORT NUMBER
NRL/JA/7330--12-1277

9. SPONSORING/MONITORING AGENCY NAME(S) AND ADDRESS(ES)
Office of Naval Research
One Liberty Center
875 North Randolph Street, Suite 1425
Arlington, VA 22203-1995

10. SPONSOR/MONITOR'S ACRONYM(S)
ONR

11. SPONSOR/MONITOR'S REPORT NUMBER(S)

12. DISTRIBUTION/AVAILABILITY STATEMENT
Approved for public release, distribution is unlimited.

13. SUPPLEMENTARY NOTES

14. ABSTRACT

The East Flower Garden Bank (EFGB), part of the Flower Garden Banks National Marine Sanctuary, is located in the northwestern Gulf of Mexico, about 185km southeast of Galveston, Texas. With a width of about 5km, the steep sided bank rises from water depths of over 100m to within less than 20m of the surface. Four acoustic Doppler current profiler (ADCP) moorings and four temperature/salinity strings were deployed around the EFGB with an additional ADCP on top of the bank for about 1 year. The main objective was to understand the ocean processes over the EFGB and to examine the importance of the topographically induced processes on shelf edge circulation on longer (e.g. days to seasonal) time scales. Currents were generally eastward over the bank in the upper water column. Eddy events occasionally reversed the eastward flow for a few days. Currents in the lower water column tended to align with the bank's bathymetry and mostly were directed offshore at the southern edge of the bank. Wind and eddy events moved both shelf and off-shelf waters over the bank, including waters from as deep as 200m through upwelling and/or mixing processes. Mixed layers changed by as much as 50m in a couple of days. Inertial currents occurred throughout the year and were often much larger than the tidal currents. Commonly, the inertial currents were strong enough to reverse the predominantly eastward current flow on time scales of less than a day. Westward propagating cyclonic eddies (often associated with anticyclonic eddies) likely connect biological activities of the EFGB with the West Flower Garden Bank. Banks such as the EFGB, with large aspect ratios and heights, strongly alter circulation and enhance exchange processes at the shelf break.

15. SUBJECT TERMS
east flower garden bank, current, mixed-layer depth, temperature/salinity, northwestern Gulf of Mexico

16. SECURITY CLASSIFICATION OF:			17. LIMITATION OF ABSTRACT	18. NUMBER OF PAGES	19a. NAME OF RESPONSIBLE PERSON
a. REPORT	b. ABSTRACT	c. THIS PAGE			William Teague
Unclassified	Unclassified	Unclassified	UU	16	19b. TELEPHONE NUMBER *(Include area code)* (228) 688-4734

Reset

Continental Shelf Research 63 (2013) 43–58

Contents lists available at SciVerse ScienceDirect

Continental Shelf Research

journal homepage: www.elsevier.com/locate/csr

Research papers

Current and hydrographic conditions at the East Flower Garden Bank in 2011

W.J. Teague [a,*], H.W. Wijesekera [a], E. Jarosz [a], D.B. Fribance [a,1], A. Lugo-Fernández [b], Z.R. Hallock [c]

[a] Naval Research Laboratory, Stennis Space Center, MS 39529, USA
[b] Bureau of Ocean Energy Management, New Orleans, LA 70123, USA
[c] QinetiQ North America, Slidell, LA 70461, USA

ARTICLE INFO

Article history:
Received 9 July 2012
Received in revised form
24 April 2013
Accepted 29 April 2013
Available online 13 May 2013

Keywords:
East Flower Garden Bank
Current
Mixed-layer depth
Temperature/salinity
Northwestern Gulf of Mexico
(27–28 N, 93–94 W)

ABSTRACT

The East Flower Garden Bank (EFGB), part of the Flower Garden Banks National Marine Sanctuary, is located in the northwestern Gulf of Mexico, about 185 km southeast of Galveston, Texas. With a width of about 5 km, the steep-sided bank rises from water depths of over 100 m to within less than 20 m of the surface. Four acoustic Doppler current profiler (ADCP) moorings and four temperature/salinity strings were deployed around the EFGB with an additional ADCP on top of the bank for about 1 year. The main objective was to understand the ocean processes over the EFGB and to examine the importance of the topographically induced processes on shelf edge circulation on longer (e.g. days to seasonal) time scales. Currents were generally eastward over the bank in the upper water column. Eddy events occasionally reversed the eastward flow for a few days. Currents in the lower water column tended to align with the bank's bathymetry and mostly were directed offshore at the southern edge of the bank. Wind and eddy events moved both shelf and off-shelf waters over the bank, including waters from as deep as 200 m through upwelling and/or mixing processes. Mixed layers changed by as much as 50 m in a couple of days. Inertial currents occurred throughout the year and were often much larger than the tidal currents. Commonly, the inertial currents were strong enough to reverse the predominantly eastward current flow on time scales of less than a day. Westward propagating cyclonic eddies (often associated with anticyclonic eddies) likely connect biological activities of the EFGB with the West Flower Garden Bank. Banks such as the EFGB, with large aspect ratios and heights, strongly alter circulation and enhance exchange processes at the shelf break.

Published by Elsevier Ltd.

1. Introduction

The general circulation of the outer Texas–Louisiana shelf has been broadly described by several investigations (Cochrane and Kelly, 1986; Cho et al., 1998; Nowlin et al., 1998, 2005). The low-frequency flow at the shelf edge was found to be generally towards the east or northeast. This flow balances the generally westward flow on the inner shelf and is the southern limb of the cyclonic gyre in the northwestern Gulf of Mexico (Cochrane and Kelly, 1986). Currents on the inner-shelf are coherent with the low-frequency, alongshelf winds (Jarosz and Murray, 2005; Cochrane and Kelly, 1986). It has been suggested that the currents in the northwestern Gulf of Mexico near the shelf edge are driven by winds (Sturges and Blaha, 1976; Blaha and Sturges, 1981), buoyancy forces, and mesoscale eddies generated directly and indirectly by rings detached from the Loop Current (LC) (Hamilton, 1992; Hamilton et al., 2002; Nowlin et al., 2005). Eastward currents at the shelf edge are thought to result from an integrated effect of anticyclonic eddies impinging on the shelf (Cochrane and Kelly, 1986; Hamilton, 1992; Hamilton et al., 2002; Nowlin et al., 2005). There could be large cross-isobath currents due to eddies. These eddy driven cross-isobath flows may even dominate the exchange across the shelf break (Nowlin et al., 2005). Oey (1995) proposed that the flow at the shelf edge was additionally modulated by the wind stress curl. Observations of temperature and salinity show that interaction of eddies with the shelf edge can advect warmer and saltier water onto the shelf while moving cooler and fresher shelf water offshore (Nowlin et al., 1998).

The Flower Garden Banks are located on the outer shelf in the northwestern Gulf of Mexico. They are far enough off the Louisiana coast to not be directly influenced by Mississippi and Atchafalaya Rivers runoff (Rezak et al., 1990), although some low-saline (30–31 psu) water has been observed near the surface and just above the coral heads at high river discharge periods (Dodge and Lang, 1983; Nowlin et al., 1998; Deslarzes and Lugo-Fernández, 2007). Flow appears to have at least two layers much of the year. Using

* Corresponding author. Tel.: +1 228 688 4734.
E-mail address: William.Teague@nrlssc.navy.mil (W.J. Teague).
[1] Present address: Coastal Carolina University, Department of Marine Science, P.O. Box 261954, Conway, SC 29528-6054.

0278-4343/$ - see front matter Published by Elsevier Ltd.
http://dx.doi.org/10.1016/j.csr.2013.04.039

current meter data from two moorings located about 5 km northeast and 11 km west of the East Flower Garden Bank (EFGB), respectively, McGrail (1983) and Halper et al. (1988) found that there is usually strong eastward flow at mid-depth (about 50 m). On the other hand, Beard (1984) observed a westward flow nearby from current data during the March–May time period. Halper et al. (1988) observed an eastward flow at the beginning of winter, but soon observed a north–south sloshing with little along-shelf eastward flow. Using historical data, Sahl (1984) found that the near bottom flow was mainly offshore. Inertial oscillations associated with the passage of hurricanes (Price, 1976; Brooks, 1983) and atmospheric cold fronts (Chen et al., 1996; Halper et al., 1988; Daddido et al., 1978) have been observed. Mid-depth currents in excess of 60 cm/s and inertial currents with amplitudes in excess of 20 cm/s were found (Halper et al., 1988). The inertial oscillations can generate the largest percentage of variance for periods between 3 and 40 h and are generally on the order of magnitude of tidal variance (Chen et al., 1996). Currents near the bottom just to the northeast of the EFGB were observed to oscillate in the north–south direction with mean flows towards the south–southeast (Halper et al., 1988). No correlation was found between the oscillations and the passage of cold fronts. In addition, changes in the general current patterns between summer and winter could not be explained by changes in the wind fields. Tidal amplitudes are small at the Flower Garden Banks (DiMarco and Reid, 1998). Hence, the currents near the shelf edge at the EFGB are complicated and are not well understood.

Characterizing the flow near the shelf edge is important for determining the exchange mechanisms between the deep ocean and the shelf. Rough bathymetric features at the edge of the shelf may impact the structure and dynamics of the circulation (Moum and Nash, 2000). The purpose of this paper is to describe the low-frequency currents at the EFGB corresponding to periods of semi-diurnal tidal frequencies and longer. Long-term measurements from December 2010 to December 2011 of current velocity, temperature, and salinity from the EFGB (Fig. 1) are analyzed to obtain a quantitative understanding of submesoscale processes

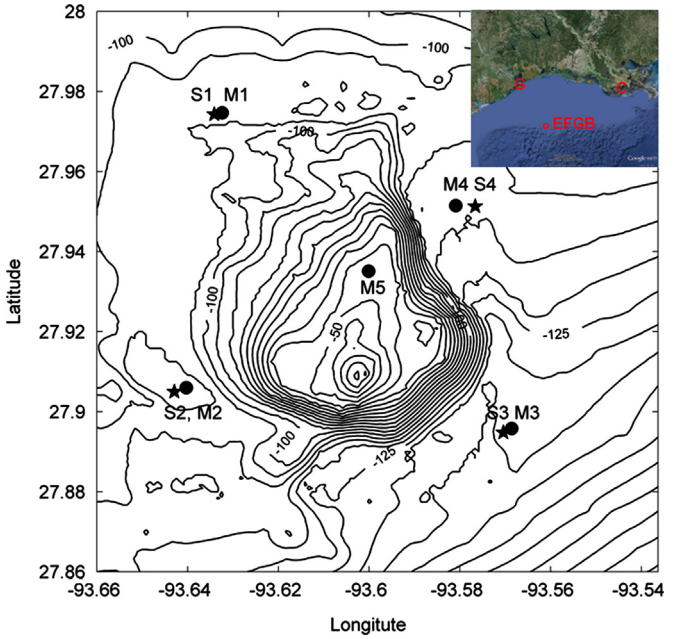

Fig. 1. Locations of MORT ADCP moorings (M1–M5; dots) and temperature/salinity strings (S1–S4; stars) are shown along with bathymetry contours (in 5-m increments) at the East Flower Garden Bank (EFGB). The inset shows the location of the EFGB in the northwestern Gulf of Mexico in relation to Galveston (G), TX and Cocodrie (C), LA.

over the EFGB and to examine the importance of topographically induced processes on shelf edge circulation on longer (days to months) time scales. The topics discussed in this paper are mainly the current and hydrographic variability and possible relationships to wind and eddy forcing. Section 2 provides some background information on the Flower Garden Banks. Section 3 provides a description of the data and instrumentation. Basic statistics of the currents are given in Section 4. A description of the current flow over and around the bank is provided in Section 5. Temperature and salinity observations from the string moorings are described and related to water mass movements and mixed layer depths in Section 6. Finally, a summary of the results is presented in Section 7.

2. Flower Garden Banks background

A series of topographic banks formed containing coral communities and coral reefs referred to as the Flower Gardens are part of a marine sanctuary designated as the Flower Garden Banks National Marine Sanctuary (FGBNMS), and are managed by the National Oceanic and Atmospheric Administration (NOAA). They are located on the Texas–Louisiana continental shelf in the northwestern Gulf of Mexico (see http://flowergarden.noaa.gov). These banks are the northernmost coral reefs in the continental United States. The footprint of the banks range from 2 km^2 to over 100 km^2 and the tops rise to within about 20 m of the sea surface from water depths of 100–150 m. The East Flower Garden Bank is part of the FGBNMS and is located about 192 km southeast of Galveston, Texas (Fig. 1). The pear-shaped EFGB is about 5 km wide and 8 km in length. Slopes are steep on the eastern and southern sides of the bank and gentle on the western and northern sides. The shallowest depth on this bank is 18 m. The surrounding waters depths are about 100 m to the west and north and about 120 m to the east and south. The EFGB is located about 20 km east of the similarly-sized West Flower Garden Bank (WFGB).

The EFGB is home to a wide array of marine life, including numerous species of rays, sharks, sea turtles and marine mammals, over 170 species of fish and approximately 300 species of reef invertebrates (Gittings, 1998). The salt dome underlying the bank has furnished the framework for coral reef development, as well as providing a reservoir for oil and gas resources. Within a 4-mile radius of the Flower Garden Banks, there are currently ten oil production platforms and there is one gas production platform within the East Sanctuary boundary. Maintaining this natural habitat is very important to the ecology of the Gulf of Mexico.

The role of the FGBs and their interactions in modifying the circulation and transport of materials is not well understood. These banks are large enough to alter the circulation on the outer shelf. Hydrodynamic processes on the reefs impact the dispersion and material transport of dissolved and particulate nutrients and of planktonic material (Wolanski et al., 1989). The extent to which bottom sediments can be resuspended and driven by strong current events and ultimately deposit contaminants onto low relief features of the banks is not known. The dynamics of current and topography interactions in controlling the dispersion of biological organisms and inorganic materials on the reefs and between the reefs are not well understood but may play a key role in reef habitat. Better understanding of the hydrodynamic processes that control material transport on reefs can provide marine managers with information necessary for the successful management of coral reefs as natural resources.

3. Data

Five ADCP moorings and four string moorings containing temperature, conductivity, and pressure (TCP) sensors were

deployed around and on top of the EFGB (Fig. 1) for a 1-year period. Locations of the ADCP moorings M1–M5 and string moorings S1–S4, and bathymetry are shown in Fig. 1. Note that M1, M2 and M4 were deployed near the same depths on the shelf (100–110 m); M3 was deployed at a depth of about 127 m, while M5 was located near the top of the bank, just to the north of the peak of the bank, at a depth of 47 m. M1–M4 were deployed just outside of the EFGB boundaries (within a couple of hundred meters). The deployment cruise was conducted from December 7–13, 2010, and utilized the R/V Pelican, out of Cocodrie, Louisiana, approximately 350 km from the EFGB. The deployment period for these moorings was six months because of anticipated biological fouling and corrosive processes, particularly for instruments located at the shallower depths. Hence, two deployments were required for the year-long measurement period. All of the moorings were successfully recovered during a Pelican cruise conducted from 26th May to 16th June of 2011. The data were downloaded, instruments were serviced and all five of the ADCP moorings and three of the four string moorings were redeployed for another 6 months, with only a gap of 1–4 days in the data. The string mooring at S1 was not redeployed due to logistical problems. Finally, all of the moorings were recovered during a Pelican cruise that was conducted from December 6 to 12 of 2011.

The ADCPs were deployed on the bottom in trawl-resistant bottom mounts that utilized dome-shaped mounting pods, called Barnys because of their barnacle-like shape (Perkins et al., 2000). Barnys are highly resistant to trawling but trawling was not a problem next to the EFGB. However the Barny's donut structure is conducive to the moorings lying flat on the bottom and hence an optimum beam orientation. The orientation is verified with an attitude sensor prior to final release of the mooring on the bottom. The Barny mounts were equipped with RD Instruments Workhorse ADCPs operating at 300 kHz (M1–M4) or at 600 kHz (M5), Sea-Bird Electronics Model 26 wave/tide gauges, and EdgeTech acoustic releases for location and recovery. During the June turnaround cruise, wave/tide gauges for M2, M4, and M5 were replaced with high-frequency pressure sensors (ppods; Moum and Nash, 2008). Ppods will be used to measure the pressure drop across the EFGB in response to the flows over the bank and topographic form drag will be estimated in a future study. The ADCPs (transducer heads situated about 0.5 m off the bottom) recorded current profiles at 2 m vertical resolution at each mooring except for a resolution of 4 m at M3 every 12 or 15 min with an accuracy of 0.5% of the water velocity over nearly the full water column. Inherent to the ADCP design, side-lobe interference with the main lobes of the acoustic beams prevented determination of the velocity within about 5–10 m from the surface (depending on the water depth). The ADCP data records were complete (approximately 6-month records for each deployment period) with the exception of the data at M5 which recorded only 41 days of data at the start of the first half of the deployment but recorded a full record for the second half of the deployment. Very little editing was required for the current data. Water temperatures were recorded within the Barny with an accuracy of 0.01 °C. The ppod and wave/tide gauge data will not be discussed here. For some of the analyses, high-frequency fluctuations (including tidal and inertial) were removed from the data by applying a low-pass filter with a 40 h half-amplitude point or cutoff frequency. The usual naming conventions are utilized: U, positive towards the east and V, positive towards the north. Table 1 provides a summary of the Barny mooring positions, time periods, sampling intervals, water depths, and instrument types.

Four TCP string mooring were deployed within about 200 m of Barny moorings at M1–M4 during the first half of the deployment and three were redeployed at M2–M4 during the second half of the mooring period. Each string contained eight to twelve sensors that recorded temperature and conductivity. Some of these also recorded pressure. The large majority of the instruments were Sea-Bird Electronics MicroCats (SBE37). Some In-Situ Aqua Trolls that recorded temperature, conductivity, and pressure were interspersed on each of the string moorings. The MicroCats sampled every 6 min with an accuracy of ± 0.002 °C and 3 μS/cm. The Aqua Trolls sampled every 12 min with lower accuracies of ± 0.1 °C and $\pm 0.5\%$ of reading+1 μS/cm. The string data were low-pass filtered (0.5 h) and resampled at 15 min intervals. Several of the conductivity sensors failed towards the ends of the deployments due to biofouling. Records that ended prematurely, but when between good records, located above and below, were vertically interpolated. TCP sensor types, nominal depths, and length of good data record from the beginning are listed in Table 2.

Meteorological wind observations were collected half-hourly at the southern edge of the EFGB at National Data Buoy Center Station 42047, and at Station 42046 located approximately 37 km west of the EFGB. Winds at 42046 were used when 42047 was out of service, which was about half of the year-long mooring period. The data at the two buoys were quite similar during concurrent recording periods. Winds are shown as a vector stick plot and as a time series plot of speed in Fig. 2. Wind velocities were smoothed using a 12-h running mean for both the speed and stick plot, but were subsampled every 6 h for the stick plot. For January through May and September through December winds were dominated by north–south changes in direction caused by passage of numerous atmospheric fronts. From May through August winds were primarily from the southwest, south and southeast with strongest winds from the southeast. Winds during the deployment period were typical for this area (Cochrane and Kelly, 1986; Gutierrez de Velasco and Winant, 1996; Walker and Hammack, 2000). Note the persistent northerly episode between days 240 and 255. Fig. 3

Table 1
ADCP mooring summary.

	Lat.	Lon.	Start day 2010/2011	End day 2011	*dt* (min)	*z*1 (m)	*zn* (m)	*dz* (m)	Depth (m)	Type (kHz)
M1-D1	27.975	−93.632	342	152	12	12	98	2	101	300
M1-D2	27.971	−93.630	153	342	15	8	91	2	98	300
M2-D1	27.906	−93.640	343	151	12	12	102	2	106	300
M2-D2	27.907	−93.640	152	342	15	11	100	2	105	300
M3-D1	27.896	−93.569	343	151	12	12	120	4	127	300
M3-D2	27.896	−93.569	152	342	15	16	116	4	127	300
M4-D1	27.952	−93.581	343	151	12	12	102	2	106	300
M4-D2	27.952	−93.581	152	342	15	11	101	2	106	300
M5-D1	27.935	−93.600	343	19	12	6	43	2	47	600
M5-D2	27.935	−93.600	152	342	15	6	43	2	47	600

Columns correspond to mooring number, latitude, longitude, start day and end day in 2010–2011, sampling interval in minutes (*dt*), depths (m) of top velocity bin (*z*1) and bottom velocity bin (*zn*), and bin interval (*dz*), water depth in m, and ADCP frequency.

Table 2
String mooring summary.

	Lat.	Lon.	Start day 2011/2011	End day 2011	Top-z (m)	Bot-z (m)	Depth (m)	No.	Type
S1-D1	27.974	−93.634	343	153	7	101	102	11	8MC, 3AT
S2-D1	27.905	−93.643	344	161	11	107	108	12	8MC, 4AT
S2-D2	27.905	−93.643	162	342	8	106	107	10	8MC, 2AT
S3-D1	27.895	−93.570	346	158	12	128	129	13	9MC, 4AT
S3-D2	27.895	−93.570	161	341	10	128	129	13	9MC, 4AT
S4-D1	27.951	−93.577	344	158	12	104	106	10	8MC, 2AT
S4-D2	27.951	−93.577	162	341	12	106	107	11	8MC, 3AT

Columns correspond to string mooring number, latitude, longitude, start day and end day in 2010–2011, top instrument level (top-z) and near-bottom instrument level (bot-z) in m, water depth in m, total number of instruments (no.), and type of instruments (and number of each type) (MC: SeaBird MicroCat; AT: In-Situ Aqua Trolls).

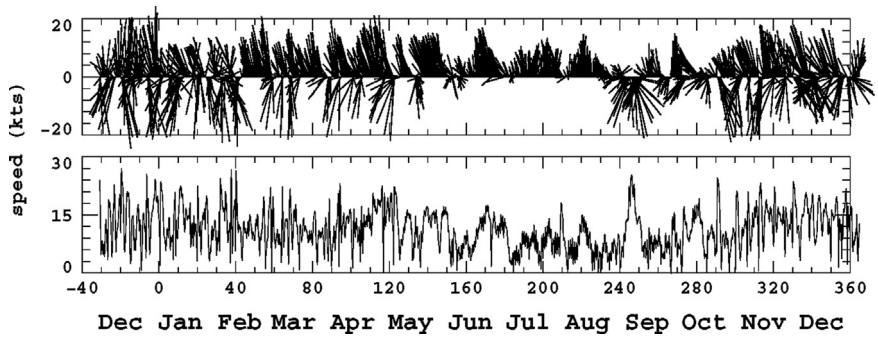

Fig. 2. Vector stick plot of winds and wind speed time series. The velocity scale for the stick plots is indicated on the y-axis; northward component is up. The x-axis shows days and months relative to 2011.

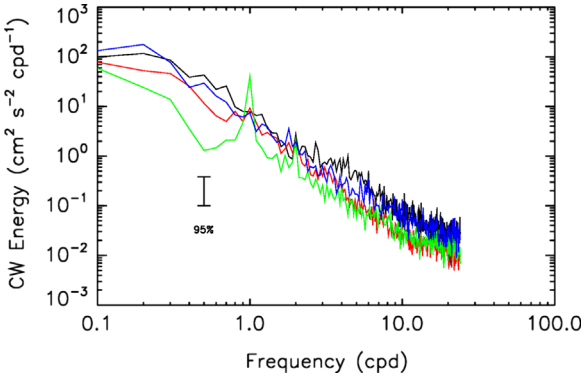

Fig. 3. Clockwise (CW) rotary autospectra of the wind data for seasons (winter, spring, summer, and fall) of the year are shown. A significant diurnal peak (green curve) is present for the summer (July–September). (For interpretation of the references to color in this figure legend, the reader is referred to the web version of this article.)

shows the clockwise (CW) rotary autospectrum of the wind data for each season: winter (January–March), etc. A significant peak in the diurnal frequency is present for the summer (July–September); low-frequency energy is lower for the summer than for the other seasons. Counterclockwise spectra (not shown) contain no peaks. The diurnal peak may be associated with a modulation of the wind field by sea breeze. Zhang et al. (2009) suggested that sea breeze can have effects as far as 300 km from the coast.

4. Statistics

Basic statistics for each ADCP mooring were computed for each half of the deployment period (mid-December 2010 through early June 2011, referred to as winter–spring, and early June 2011 through early December 2011, referred to as summer–fall) from the low-pass filtered data. Statistics for the top, several mid-level, and bottom velocity bins are shown in Table 3. The standard error listed here is defined as the standard deviation divided by the square root of the number of degrees of freedom, which is estimated as the sample period divided by the integral time scale. The integral time scale is defined as the discrete integral of the time-lagged autocorrelation function from zero lag to the first zero crossing after demeaning and detrending the time series.

Integral time scales during winter–spring for the U velocity component (omitting M5, due to the short record) generally were about 1–2 weeks in the upper water column and less than a week in the lower water column and near the bottom, except for at M1, where time scales were longer throughout the water column. Periods of stronger eastward flow that occurred during the winter–spring period were less interrupted by the bank at M1 due to its location on the north side of the bank and resulted in these longer time scales. Time scales for the V component were generally less than a week but were sometimes longer near the bottom for V than for U. Integral time scales during the summer–fall period for the U component were generally longer than for winter–spring near the surface (10–20 days) and somewhat shorter, from 2 to 5 days, near the bottom. Shorter time scales, mostly less than 5 days, for the V component throughout the water column were similar to those in the winter–spring period. The shorter time scales for the V component were related to the on and off shelf flows along the topography, perhaps influenced by shelf waves. The longer time scales for the U component corresponded primarily to periods of strong east–west velocity in the upper water column. Similar integral time scales were found in the northeastern Gulf of Mexico (Teague et al., 2006; Carnes et al., 2008) and for the alongshelf currents in the northwestern Gulf of Mexico (Nowlin et al., 2005).

East–west velocity components were generally larger than the north–south components. The maximum current speed observed over the entire deployment was 59 cm/s (at M3 near the surface) directed towards the east–northeast. The maximum current speed

Table 3
Basic statistics over the winter–spring (D1) and summer–fall (D2) periods for selected depth levels. Columns correspond to mooring, measurement depth z, average current component $\overline{U}$, standard deviation σ_U, standard errors SE_U, minimum U value U_{min}, maximum U value U_{max}, and similarly for V, maximum speed S_{max}, direction of the maximum speed D_{max}, integral time scales IT_U and IT_V, mean kinetic energy MKE and mean eddy kinetic energy EKE. Units are cgs.

	z	$\overline{U}$	σ_U	SE_U	U_{min}	U_{max}	$\overline{V}$	σ_V	SE_V	V_{min}	V_{max}	S_{max}	D_{max}	IT_U	IT_V	MKE	EKE
M1-D1	12	13.76	10.49	2.35	−18.11	41.49	1.11	5.05	0.76	−12.47	23.06	41.5	91.02	8.59	3.9	95.35	67.73
M1-D1	20	13.13	10.02	2.46	−18.21	37.54	0.47	5	0.77	−14.29	21.55	37.54	90.92	10.34	4.08	86.37	62.67
M1-D1	40	12.04	9.25	2.85	−12.76	35.32	0.47	4.39	0.69	−14.25	17.16	35.36	93.11	16.25	4.22	72.65	52.39
M1-D1	60	9.83	9.23	3.01	−16.89	32.86	1.43	3.99	0.62	−10.21	15.39	32.95	94.37	18.18	4.13	49.38	50.59
M1-D1	80	5.72	7.75	2.18	−16.5	25.77	2.24	3.67	0.41	−8.67	14.54	26.99	72.46	13.48	2.16	18.9	36.74
M1-D1	98	3.45	6.39	1.95	−15.48	14.08	3.08	4.25	0.97	−5.95	16.45	21.35	39.8	15.98	8.91	10.69	29.43
M2-D1	12	14.57	10.32	2.02	−11.52	38.49	0.35	6.3	1.02	−21.38	23.08	38.71	96.14	6.5	4.45	106.22	73.11
M2-D1	20	13.87	9.78	2.02	−12.08	37.47	−0.3	6	1	−18.88	21.04	38.45	102.99	7.29	4.7	96.28	65.78
M2-D1	40	12.16	8.4	1.82	−10.53	32.19	−0.93	5.6	0.89	−16.11	16.51	33.68	113.5	8.03	4.3	74.34	51.02
M2-D1	60	8.7	6.71	1.78	−9.48	26.68	−1.38	5.91	0.8	−14.42	17.02	27.08	99.95	11.96	3.16	38.77	39.98
M2-D1	80	3.61	4.11	0.95	−9.72	16.76	−2.06	6.16	0.88	−17.17	20.65	21.71	341.88	9.12	3.51	8.62	27.45
M2-D1	100	1.5	2.52	0.47	−13.73	7.36	−2.32	4.95	0.91	−15.52	14.62	19.91	316.8	5.8	5.74	3.81	15.43
M2-D1	102	1.68	2.83	0.55	−13.66	9.47	−2.05	4.49	0.82	−13.59	13.6	19.14	314.84	6.44	5.67	3.5	14.08
M3-D1	12	12.38	10.33	2.44	−14.75	35.89	−0.51	5.59	0.83	−16.84	18.07	36.65	107.17	9.55	3.81	76.76	68.92
M3-D1	20	11.46	9.55	2.25	−14.27	33	−0.82	5.19	0.77	−17.03	15.53	33.78	116.58	9.5	3.79	66	59.04
M3-D1	40	8.98	8.16	1.9	−11.41	30.08	−0.34	4.27	0.61	−12.81	14.14	30.84	68.86	9.24	3.45	40.35	42.42
M3-D1	60	4.72	8.11	1.66	−12.5	28.06	−0.1	4.73	0.62	−17.48	12.35	30.65	66.25	7.19	2.91	11.15	44.11
M3-D1	80	0.83	7.05	0.99	−16.92	22.2	−0.99	5.76	1.04	−20.67	12.53	25.33	60.95	3.39	5.61	0.83	41.45
M3-D1	100	−2.07	4.89	0.73	−14.83	13.69	−2.69	6.4	1.36	−22.78	13.49	24.34	200.66	3.81	7.76	5.77	32.42
M3-D1	120	−1.84	3.22	0.61	−10.7	6.61	−2.75	5.93	1.31	−21.1	14.64	22.68	201.55	6.08	8.34	5.47	22.75
M4-D1	12	12.68	9.99	2.16	−17.78	37.56	−1.38	5.56	0.81	−18.57	18.24	37.7	94.92	8.01	3.62	81.32	65.39
M4-D1	20	11.78	9.33	2.21	−17.32	36.41	−1.88	5.56	0.82	−18.3	15.44	36.6	95.94	9.59	3.74	71.19	58.99
M4-D1	40	11.35	8.48	2.65	−11.42	30.65	−2.47	4.69	0.92	−18.01	10.73	32.35	118.19	16.66	6.54	67.47	46.93
M4-D1	60	8.2	6.41	1.98	−8.3	28.32	−1.53	4.18	0.74	−13.35	9.01	28.79	100.77	16.28	5.39	34.81	29.31
M4-D1	80	1.69	4.69	1.02	−7.2	21.72	−0.84	5.08	0.76	−15.46	12.6	23.1	111.21	8.01	3.86	1.77	23.91
M4-D1	100	−1.29	1.57	0.19	−5.65	5.54	−0.7	4.68	0.8	−14.16	11.69	14.16	179.84	2.54	5.02	1.07	12.18
M4-D1	102	−1.08	1.53	0.17	−5.8	3.39	−0.74	4.32	0.76	−13.79	10.36	13.83	184.2	2.06	5.34	0.85	10.5
M5-D1	6	19.94	11.61	2.91	−8.36	45.79	2.34	4.49	0.85	−11.75	15.12	46.36	81	2.39	1.37	201.6	77.44
M5-D1	20	20.05	11.17	2.93	−7.75	45.65	0.02	3.98	0.73	−12.48	14.66	45.69	92.18	2.6	1.28	200.99	70.33
M5-D1	40	17.17	8.97	2.44	−6.42	37.16	1.02	3.06	0.57	−5.72	13.11	37.27	94.46	2.81	1.3	148	44.94
M5-D1	44	13.84	6.63	1.84	−4.61	28.9	2.23	2.69	0.54	−2.38	11.27	28.94	92.73	2.93	1.53	98.27	25.63
M1-D2	7	5.89	13.28	3.16	−35.76	41.82	1.32	8.39	1.21	−25.55	29.99	42.14	82.92	10.48	3.84	18.25	123.35
M1-D2	21	5.31	12.53	3.06	−37.29	36.70	−0.01	7.59	1.01	−23.24	28.96	38.43	254.42	11.07	3.26	14.12	107.26
M1-D2	41	3.93	11.50	3.08	−26.14	32.74	0.40	5.91	0.87	−15.40	23.30	32.95	83.36	13.34	3.98	7.80	83.65
M1-D2	61	2.99	9.96	1.72	−30.15	24.49	1.95	4.44	0.66	−13.35	13.91	30.18	272.57	5.54	4.16	6.37	59.44
M1-D2	81	1.55	7.43	1.01	−22.61	24.57	1.73	3.85	0.47	−11.52	15.73	28.22	59.43	3.40	2.74	2.71	35.02
M1-D2	91	0.80	5.96	0.78	−22.87	17.77	2.87	4.50	0.48	−10.39	24.92	30.57	35.46	3.22	2.15	4.44	27.87
M2-D2	10	7.10	12.99	3.76	−31.61	46.90	0.71	8.72	1.41	−20.88	33.94	47.31	70.16	15.72	4.92	25.48	122.36
M2-D2	20	6.14	12.88	3.97	−29.41	46.97	−0.12	8.42	1.33	−20.33	33.71	47.02	87.02	17.80	4.65	18.84	118.41
M2-D2	40	4.28	9.85	3.25	−26.79	35.51	0.35	7.03	1.09	−15.32	38.21	39.05	345.41	20.46	4.51	9.23	73.18
M2-D2	60	1.62	5.75	1.35	−23.01	17.44	0.88	6.21	1.07	−14.57	27.50	33.32	324.20	10.31	5.53	1.71	35.81
M2-D2	80	1.14	3.33	0.47	−11.24	8.93	−1.50	5.74	0.90	−12.86	17.31	19.68	331.23	3.78	4.65	1.76	22.01
M2-D2	100	1.69	1.73	0.20	−2.61	8.01	−1.33	2.61	0.31	−8.89	6.20	11.59	137.40	2.56	2.62	2.32	4.89
M3-D2	16	5.44	13.46	3.94	−30.68	52.89	−0.24	8.49	1.23	−20.47	34.75	59.21	63.13	16.02	3.95	14.82	126.61
M3-D2	20	5.11	13.42	4.00	−29.20	53.34	−0.37	8.34	1.21	−19.89	33.71	59.48	63.46	16.54	3.94	13.11	124.89
M3-D2	40	2.63	10.63	3.19	−24.58	40.17	−0.73	6.96	1.13	−16.16	28.35	40.19	88.47	16.83	4.95	3.73	80.75
M3-D2	60	−1.67	7.87	1.11	−20.36	27.18	−2.24	7.72	1.18	−23.84	25.27	28.61	214.30	3.71	4.37	3.92	60.82
M3-D2	80	−2.30	5.96	0.81	−14.42	18.17	−3.46	7.65	1.10	−25.31	14.75	28.29	206.65	3.43	3.83	8.63	46.99
M3-D2	100	−2.20	4.91	0.68	−15.44	11.11	−3.01	6.83	0.98	−25.92	16.71	30.14	210.70	3.56	3.82	6.97	35.35
M3-D2	116	−1.85	4.25	0.61	−17.29	13.29	−1.52	5.43	0.69	−27.08	20.35	32.12	212.54	3.81	3.04	2.86	23.78
M4-D2	11	5.11	12.05	3.13	−30.73	32.83	0.64	7.50	1.05	−18.46	34.33	35.78	116.02	12.61	3.65	13.27	100.69
M4-D2	21	5.20	12.01	3.31	−29.54	33.59	−0.13	7.31	1.02	−22.30	29.64	37.71	117.12	14.21	3.62	13.54	98.78
M4-D2	41	5.23	11.50	3.20	−24.41	32.78	−0.32	5.79	0.90	−17.40	25.51	32.93	95.49	14.42	4.50	13.74	82.90
M4-D2	61	2.92	5.90	0.82	−20.26	19.14	0.15	5.38	0.89	−15.15	21.67	22.62	342.77	3.61	5.14	4.28	31.84
M4-D2	81	−0.85	3.04	0.44	−9.63	10.43	0.67	4.32	0.58	−10.56	11.51	13.41	130.26	3.84	3.34	0.59	13.96
M4-D2	101	−1.33	1.22	0.15	−5.38	2.90	0.53	3.47	0.43	−9.57	13.26	13.52	348.67	2.74	2.81	1.02	6.76
M5-D2	6	6.95	13.64	2.29	−32.18	41.38	0.54	8.95	1.43	−27.93	40.85	46.15	118.25	5.26	4.75	24.31	133.04
M5-D2	20	5.60	12.65	3.58	−31.87	38.74	−0.99	7.85	1.22	−25.15	34.15	42.92	122.26	14.98	4.47	16.18	110.88
M5-D2	40	6.16	11.72	3.38	−26.40	32.03	1.42	6.47	1.10	−17.25	23.19	32.44	99.69	15.56	5.43	19.98	89.61
M5-D2	44	5.91	10.31	2.99	−19.09	29.16	2.91	5.47	1.07	−11.04	18.52	31.10	65.90	15.70	7.09	21.71	68.10

observed on top of the bank was 46 cm/s (near the surface) during both deployment periods. Average east–west velocity components generally decreased with depth while average north–south components often increased with depth. For moorings located off the bank, the maximum southward current velocity of −27 cm/s occurred near the bottom at M3. Standard deviations of U and V generally were of the same order or greatly exceeded the mean values. Hence, the means were often not well defined.

Mean eddy kinetic energy (EKE) off the bank for the winter–spring period ranged from a low of about 10 cm^2/s^2 near the bottom at M4 to a high of 73 cm^2/s^2 near the surface at M2, while on top of the bank at M5 mean EKE ranged from 26 to 78 cm^2/s^2. During summer–fall, mean EKE off the bank ranged from 5 cm^2/s^2 near the bottom at M2 to 127 cm^2/s^2 at M3, while EKE ranged from 68 to 133 cm^2/s^2 on top of the bank at M5. Mean kinetic energy (MKE) off the bank for winter–spring ranged from less than 1 cm^2/s^2

at M4 to 106 cm^2/s^2 at M2. On top of the bank at M5 (short record) MKE ranged from 98 cm^2/s^2 to 210 cm^2/s^2. MKE off the bank for summer–fall ranged from less than 1 cm^2/s^2 at M4 to 25 cm^2/s^2 at M2, while on top of the bank MKE ranged from 16 to 24 cm^2/s^2. EKE was dominant during summer–fall period while MKE was more dominant during winter–spring due to stronger east–west mean flows. The observed EKEs are similar to those observed near the shelf break in the northeastern Gulf of Mexico, but the MKEs are generally more than twice as large as those observed in the northeastern Gulf (Teague et al., 2006; Carnes et al., 2008). The larger MKE values observed here are due to the dominant eastward flows.

Compass rose plots are shown for near surface and near-bottom velocities in Fig. 4. Compass rose plots provide an angle histogram of the distribution of current speed and direction along the 16 compass points (every 22.5°). The length of each bin reflects the percentage of the number of observations in that direction and the color bar indicates the magnitude of the current speed distribution. For the winter–spring period the roses for the near surface currents (M1–M4; M5 not shown due to the short record)

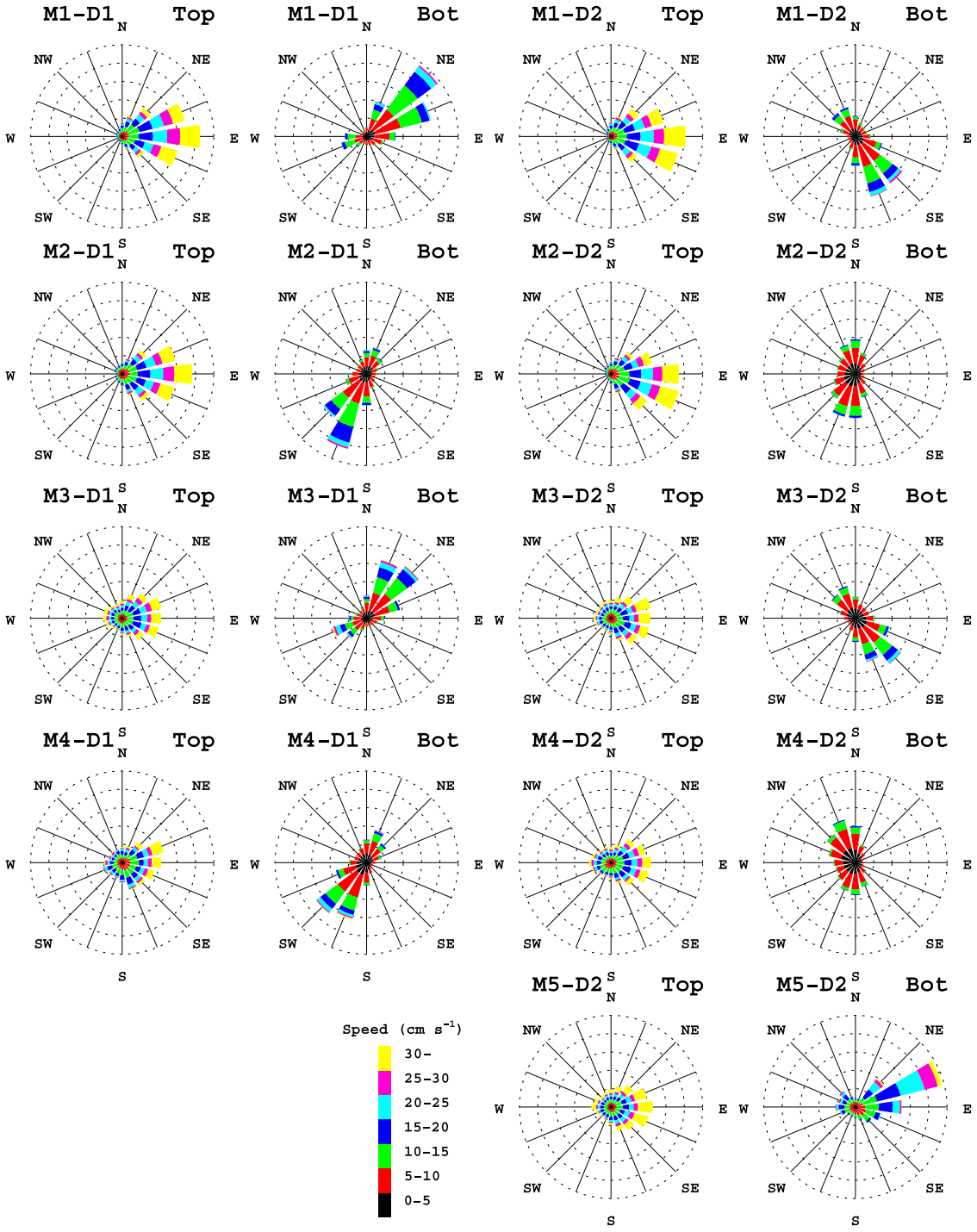

Fig. 4. Compass rose diagrams for the near-surface and near-bottom currents are shown for each ADCP mooring, except for M5-D1 (short record) for each deployment period (D1: deployment 1, winter–spring; D2: deployment 2, summer–fall). The current directions are distributed along the 16 compass points (every 22.5°), where the length of each bin provides the percentage of the number of observations in that direction and the color indicates the magnitude of the current. Dashed rings are every 5%, with the outermost ring representing 25%. Currents are plotted in the direction of the flow.

show eastward flow with the large majority of the flow between NE and SE and at least some currents in all directions. At mid-depths (excluding M5) currents began to align with the bathymetry (not shown). Roses for near the bottom show the currents aligning with the bathymetry, primarily offshore at M2 and M3 but a significant percentage of currents are also directed onshore. For the summer–fall period currents near the surface are also mostly eastward but were more evenly distributed in all directions. Deep currents for the summer–fall period are distributed similarly to the winter–spring period. However, the full record for M5 shows primarily eastward flow with some reversals.

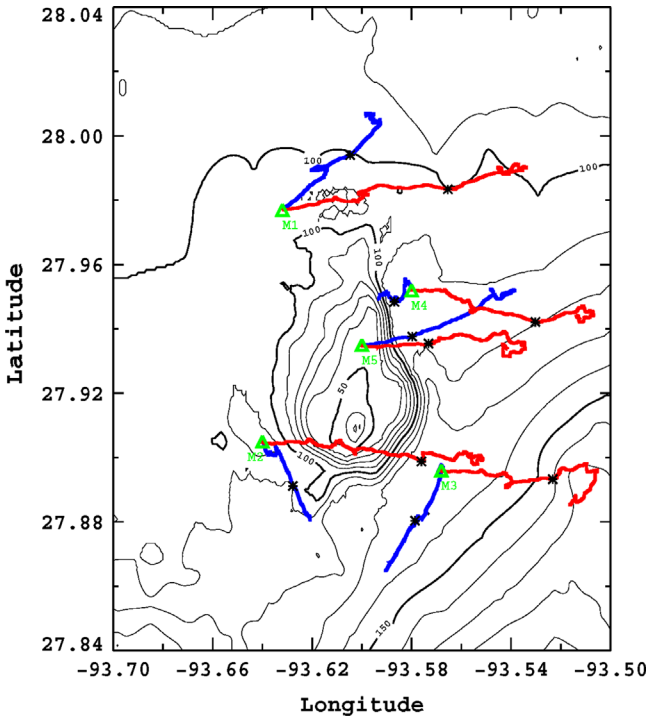

Fig. 5. Progressive vector diagrams (pvds) for each ADCP mooring are shown for both the winter–spring period and for the summer–fall period. Red lines represent pvds for average velocities for the upper 80 m for M1–M4 and upper 40 m for M5. Blue lines represent the pvds for the lower layers above the bottom. Asterisks mark the end of the winter–spring period and start of the summer–fall period. (For interpretation of the references to color in this figure legend, the reader is referred to the web version of this article.)

For further illustration, progressive vector diagrams (pvds) were computed for two layers for both deployment periods (Fig. 5; note that the pvd for M5 for the winter–spring period is only for the first 41 days). Velocities were averaged from approximately 80 m depth to near the surface for the top layer and from about 80 m to near bottom for the bottom layer, except for at M5 where the layer depth was 40 m. The pvd for the winter–spring period shows the predominately eastward flow in the top layer (red lines) and flow more aligned with the bathymetry in the bottom layer (blue lines). Compass rose plots show that although the bulk of the bottom layer flow was directed offshore, there are periods when it was onshore. The pvds indicate that the cumulative deep flows were strongest at M1 and M3. More off-shelf flow was found at M3 than at M2. At M4 the bottom layer flowed back toward the bank and then probably along the bathymetry. The kinks in the pvds occurring about midway in the winter–spring period, primarily in the upper layer, may be indicative of eddy processes over the bank. In addition, the pvds for the upper layer show mainly eastward flow until late in the summer–fall period, when the currents turned clockwise, suggesting a stronger eddy event.

5. Currents

Temporal means and principal variability ellipses (which express the variability about the means) were computed for each ADCP, for the entire period of the experiment. Ellipse parameters are presented as profiles of mean current speed and direction along with profiles of ellipse major/minor axes and ellipse

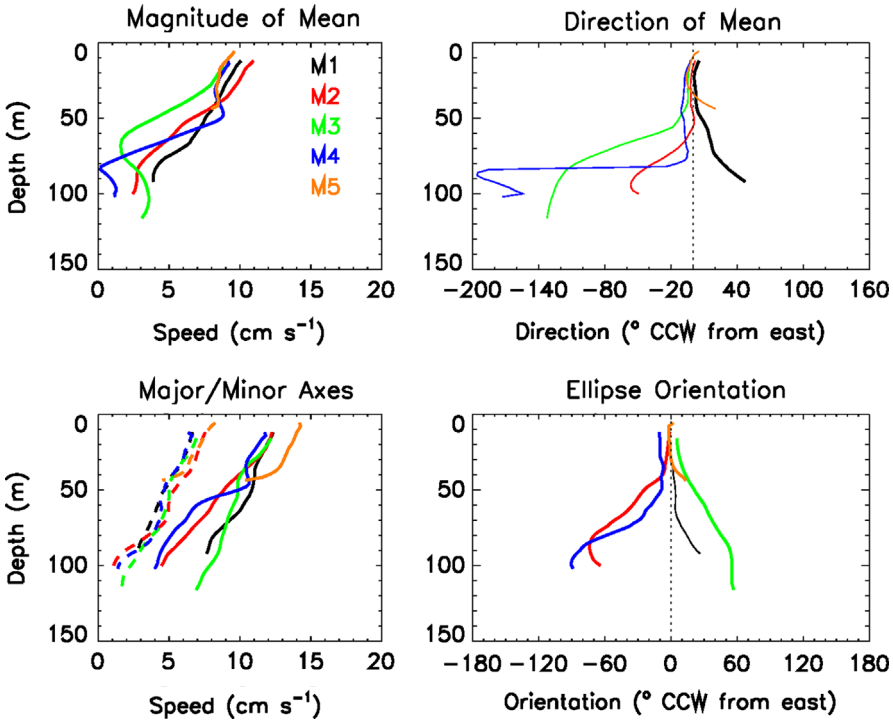

Fig. 6. Magnitudes and directions of mean velocity (upper); major and minor (dashed) axes and orientations of principal ellipses (lower) for the entire deployment period.

orientation, as functions of depth in Fig. 6. An ellipse centered on the tip of the vector representing the mean current velocity, reflects the area that is within one standard deviation of the mean. Higher variabilities, indicated by the major axes of the ellipses, are generally in the direction of the mean flows. Speeds of the means were similar and generally decreased with depth. At M3 there was a local speed minimum of about 2 cm/s near 70 m depth and a maximum of about 4 cm/s near 100 m depth. Directions of the means shallower than 70 m were nearly eastward. The variability ellipse axes generally decreased linearly with depth with major to minor axis ratios of about 2:1. Near the surface, ellipse orientations were essentially east–west. Below about 40 m orientations for M1 and M3 rotated CCW with depth from E–W to about SW–NE; for M2 and M4 orientations rotated CW to about NW–SE. The near-bottom ellipse orientations for M1–M4 are thus aligned with local bathymetry. Orientations for M5 remained close to zero (E–W), being confined to the upper 50 m. The major axes are essentially standard deviations of speed along an axis in the orientation direction, and provide a rough measure of uncertainty for the mean profiles. Hence, deeper than about 70 m, mean speeds were significantly lower than the major axis profiles and corresponding directions (of the means) were more unreliable.

Monthly averages of U and V component profiles are presented in Fig. 7. The U component dominated except for October–December where V components had similar magnitudes to U components. Lowest velocities occurred in March. Sometimes there were fairly constant velocity layers near the surface. Layers of near constant velocity also occurred near the bottom. Velocity-shear gradient layers that extended from near the surface to near the bottom occurred in February and March, and between the surface and bottom layers when present. Subsurface velocity minima and maxima occurred throughout the water column. U components were eastward in the upper water column except for October and November. V components were generally small in both directions, except for during October to December, where the V components were directed mainly southward and were similar in magnitude to the U component. Cross-shelf exchange could have occurred during this time period. Largest average velocities were not confined to the top of the bank.

Sections of low-passed filtered (40 h) U and V velocity components as a function of time and depth are shown for each of the Barny moorings in (a; U component) and in Fig. 8(b; V component). Eastward flows along the shelfbreak dominated the circulation pattern. There were periods of westward flow during March (days 60–80), October (days 270–300), and November (days 310–330). The westward flows can perhaps be attributed either to small cyclonic eddies that were generated from processes associated with a nearby LC Ring or by storm events. Vorticity computed between currents at M2–M4 (Fig. 9) displayed large positive peaks (near days 60, 280, and 330) for westward-flow time periods and are suggestive of cyclonic eddies. Sea-surface heights (SSHs) from altimetry suggested that the LC extended well into the northern Gulf during October, 2011. However, temporal resolution of the altimetry tracks of about 10 days and spatial resolutions of the tracks of about 7 km along track and tens of kilometers between tracks were not adequate in resolution to resolve eddies with diameters on the order of 10 km.

SSHs and sea-surface temperatures are assimilated by NRL's Intra-Americas Sea Nowcast/Forecast System (IASNFS) (Ko et al., 2008). Hence, the model can provide a reasonable broad picture of the eddy field. Currents and temperature at 50 m depth from this model are shown in Fig. 10 for October 18, 2011 (day 290). The LC extended well into the Gulf of Mexico (edge is shown in Fig. 10 at about 26°N and 88°W) with a detached anticyclonic warm core ring near 25°N and 92°W. There are a series of anticyclones and cyclones depicted by the model between the LC and the detached warm ring. The model resolved a small cyclonic eddy depicted south of the EFGB and north of the warm ring (approximately at 27.7°N and 93.5°). The horizontal scale of the eddy was on the order of 50 to 75 km. The eddy remained in the vicinity of the bank for about two weeks. The IASNFS was used

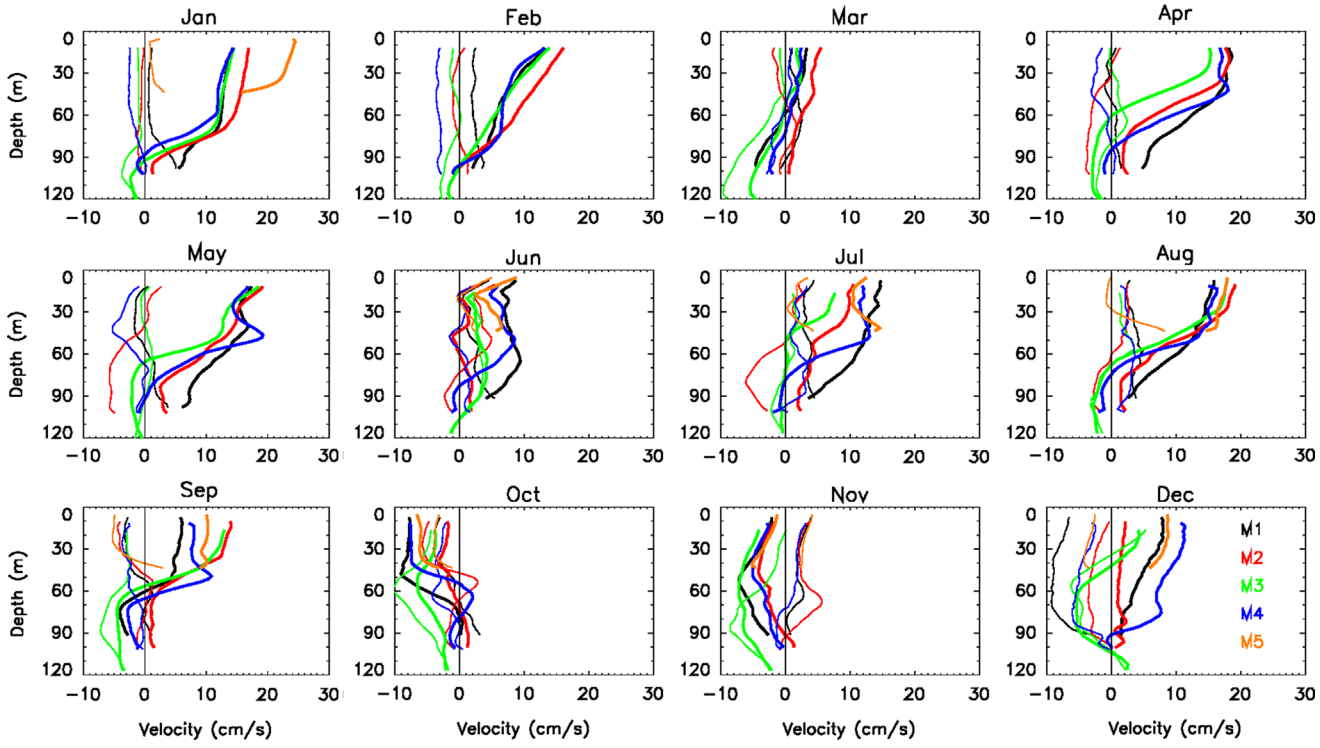

Fig. 7. Average velocity profiles for U (thick lines) and V (thin lines) are shown for each month. Colors represent the individual ADCP moorings, indicated in the December frame.

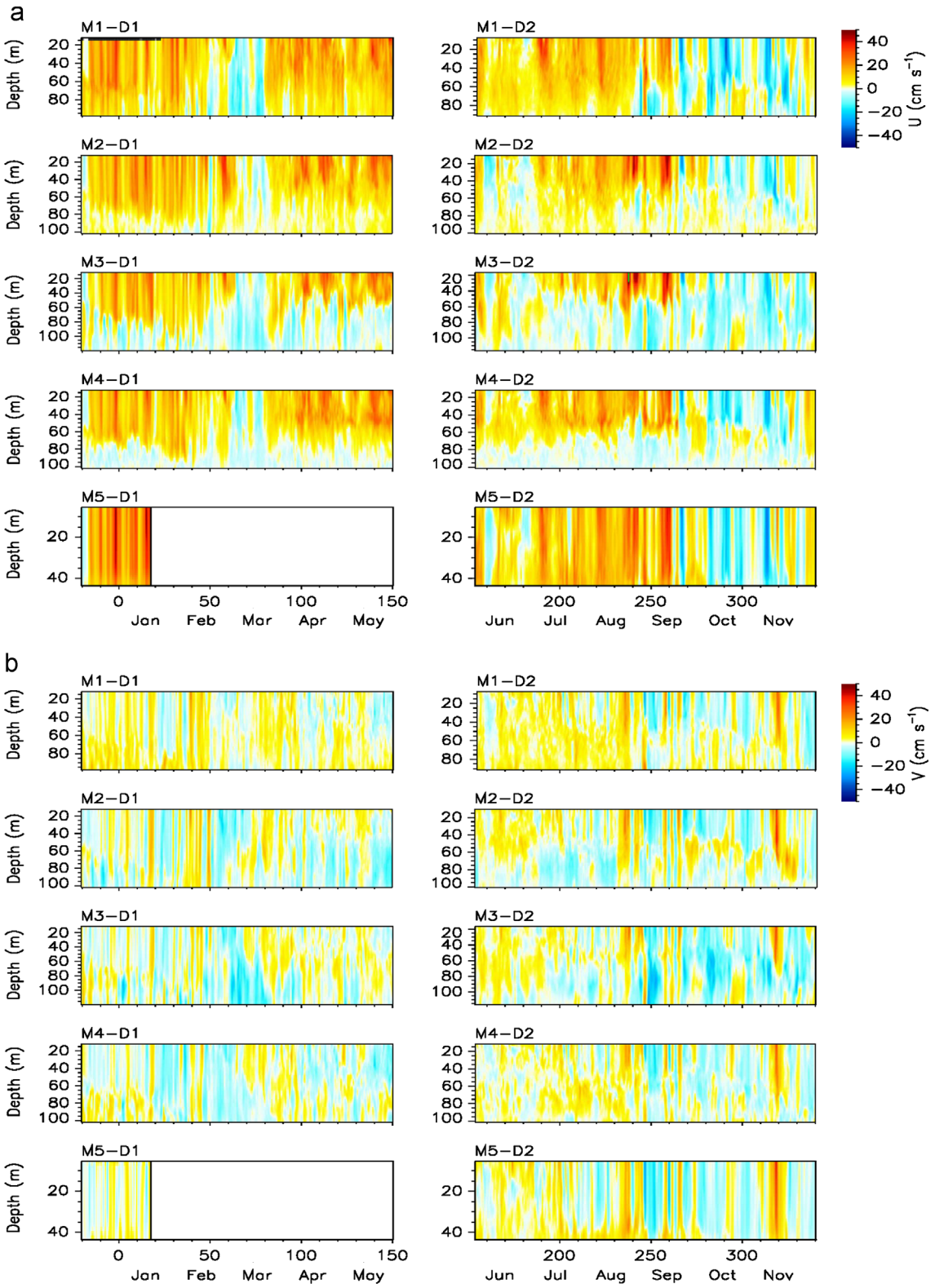

Fig. 8. (a) Velocity time series for the U (east–west component) and (b) V (north–south) component. Tides and inertial oscillations have been removed using a low-pass filter with a 40-h cutoff frequency. The *x*-axis shows days and months relative to 2011.

here to provide a perspective on the larger scale circulation at the time and to suggest what processes impacted those around and on the EFGB. A very similar pattern of cyclonic and anticyclonic eddies were also revealed in SSH data (posted at http://www.esl.lsu.edu). The cyclonic eddy appeared larger in the SSH data than in the model depictions. The main advantage of the model is that the current patterns are revealed.

The 3 major tidal components in this region are M2, K1, and O1 (DiMarco and Reid, 1998) which have periods of 12.42, 23.93, and 25.82 h, respectively. Our measurements revealed amplitudes of

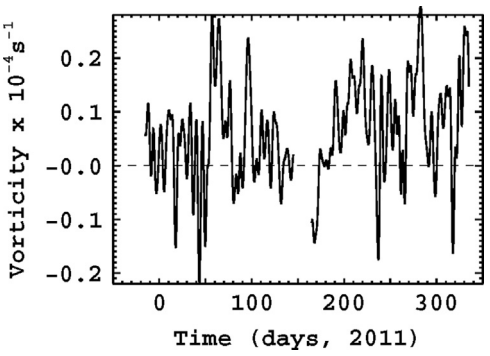

Fig. 9. Current vorticity computed, with currents low-passed at 5 days, between current observations at M2, M3, and M4. Large positive vorticity values may be indicative of cyclonic eddy patterns.

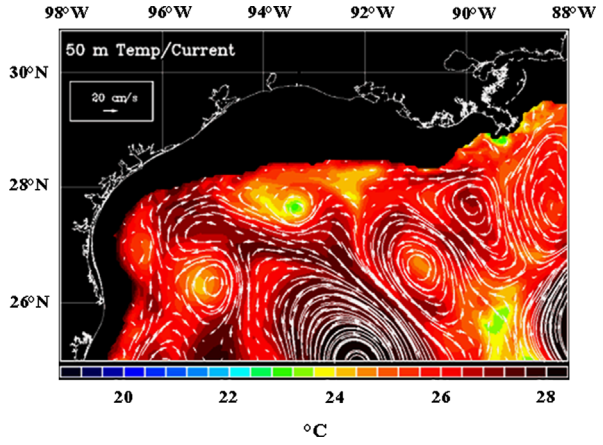

Fig. 10. Snapshot of a possible current scenario from the Intra-Americas Sea Nowcast/Forecast System (IASNFS) for October 18, 2011. Arrows indicate the current velocity and direction and the colors indicate temperature, both for 50 m water depth. A LC ring is approximately at 25°N, 92°W and a cyclonic eddy, near the EFGB, is at 27.7°N, 93.5°W.

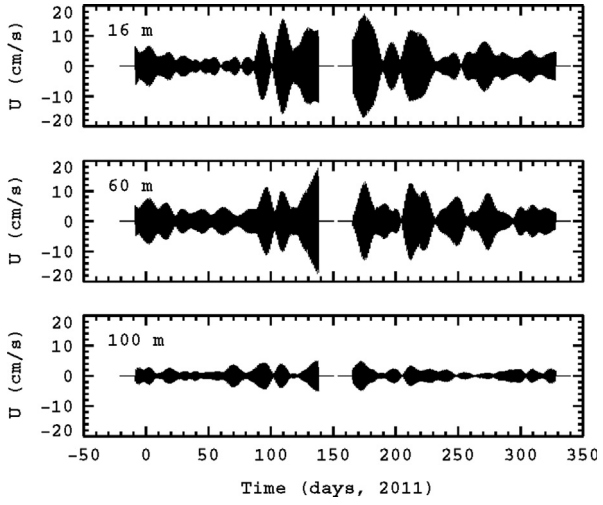

Fig. 11. Inertial band currents (east–west) at M3 for 16 m, 60 m, and 100 m. The inertial period is 24.58 h.

these tides ranging between 3 and 5 cm/s, similar to the findings of DiMarco and Reid (1998). The inertial period at the EFGB is approximately 25.58 h, which is near the O1 period. Intense inertial oscillations were found from April through August (days 90–230) (Fig. 11). Amplitudes of the inertial oscillations were often larger than tidal amplitudes and exceeded 15 cm/s. Inertial amplitudes could be modified by diurnal tides, depending on the phase difference. However, the amplified inertial amplitudes occurred mainly during summer months and were likely associated with a near-resonant response to sea breeze (Zhang et al., 2009; Jarosz et al., 2007), as evidenced by the peak during summer in the CW rotary wind autospectrum (Fig. 3). The generally observed eastward flow was reversed towards the west during this period when the amplitudes of the inertial oscillations exceeded the background eastward flow. Since the reversals may only last a few hours, they were not resolved in the plot of the filtered velocity sections (Fig. 8). The direction of the V component of velocity, reflective of on-shelf and off-shelf flow, was greatly affected by the inertial oscillations, as reversals in V occurred throughout the entire deployment period.

The contribution of the inertial, diurnal tide, and higher frequency kinetic energies (referred to as HFE) is shown by the ratio of HFE to total current kinetic energy in Fig. 12. The HFE is computed from the square of the total currents minus the 40-h low-passed currents. The HFE ranged from about 20–40% of the total energy in the upper 40 m to about 30–80% of the total energy in the lower water column, and was often near maximum close to the bottom. Interestingly, the ratio of HFE to total kinetic energy was largest at moorings M2 and M4. The lower ratio in the upper water column may be reflective of the more dominant wind driven circulation while the higher ratio in the lower water column may indicate relatively stronger inertial and diurnal tide contributions. The presence of the bank likely drives this distribution of energy.

Current vector stick plots for near bottom levels at M1–M5 were computed from the 40-h low-passed data (subsampled every 12 h), and are shown in Fig. 13. Visual inspection of these plots suggests the presence of continental shelf waves at M1–M4. Shelf waves have frequencies less than the local inertial frequency and wavelengths much greater than the water depth. They have been observed through analyses of pressure and current records (Mooers and Smith, 1968; Cutchin and Smith, 1973; Gill and Schumann, 1974; McGrail and Carnes, 1983; Halper et al., 1988). Current fluctuations due to shelf waves can be comparable to or larger than fluctuations due to tides (Kubota, et al., 1981). Some of the forcing mechanisms for the generation of shelf waves include tropical cyclones, winds, atmospheric pressure fluctuations and tides. The spectrum for the V component of velocity for M3 near the bottom is shown in Fig. 14. The semi-diurnal tide and diurnal tide/near inertial bands are clearly represented by sharp peaks in the spectrum. In addition, there are two broader peaks, at 60 and 96 h, which may be related to the shelf waves. The largest non-tidal peak (96 h) occurs in the V component, the component directed cross-shelf. Correspondingly there is a broad peak in the spectra for the U component of the winds between 48 and 120 h

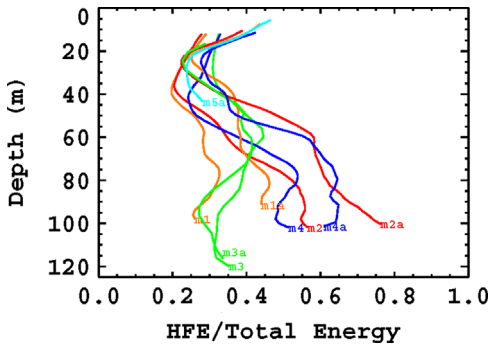

Fig. 12. Vertical profiles of the ratio of higher frequency current energies (HFE; tidal, inertial, and higher frequencies) to the total current energy. Moorings for the winter–spring period are denoted by M1–M5 and for the summer–fall period by M1a–M5a.

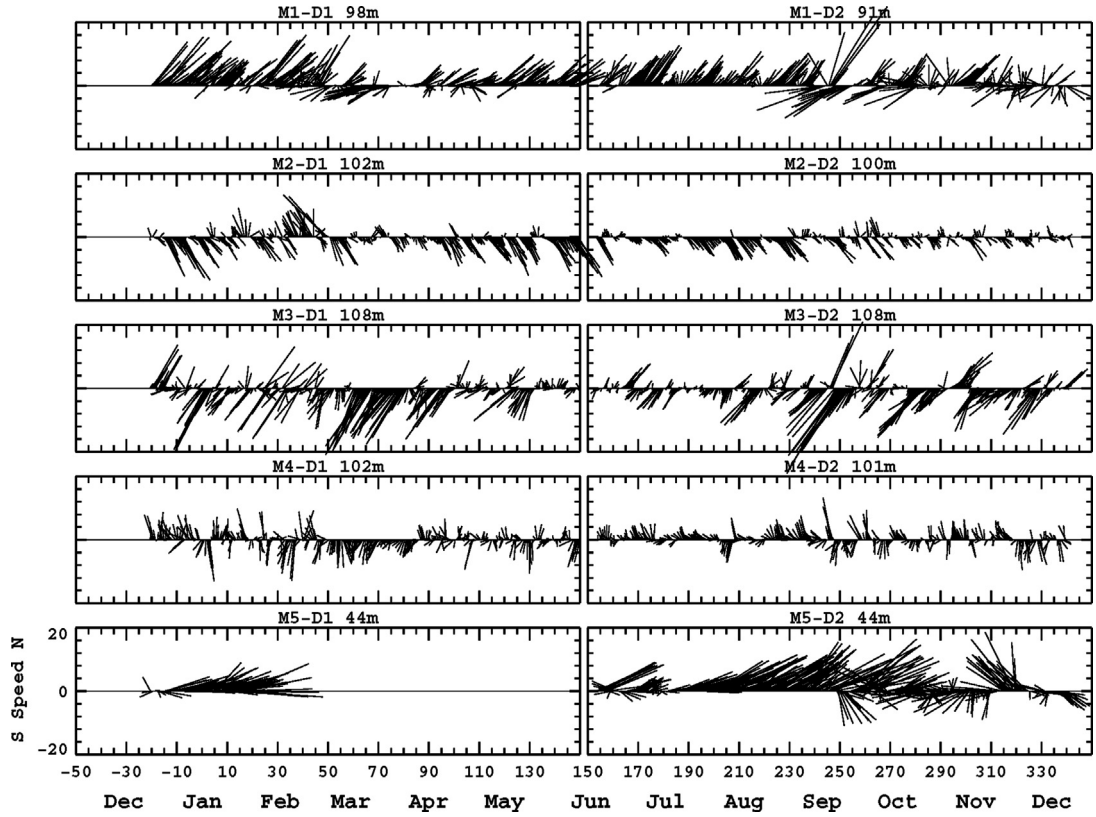

Fig. 13. Current stick vectors for the near-bottom for each mooring. Northward is along the positive *y*-axis. The *x*-axis shows days and months relative to 2011.

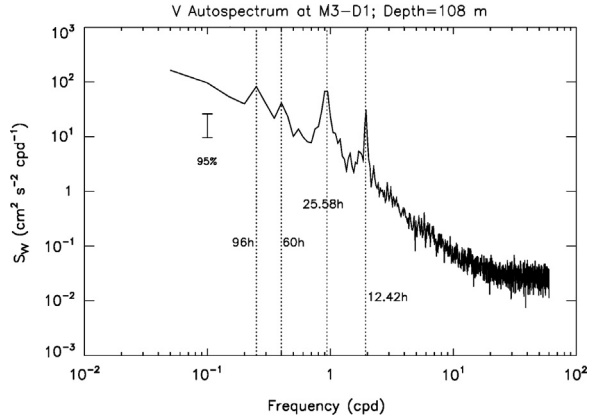

Fig. 14. Autospectrum for the V velocity component near the bottom; 60 h and 96 h periods (typical for shelf waves), inertial (25.58 h), and the M2 tide period (12.42 h) are indicated by vertical dotted lines.

(spectra not shown) suggesting that the shelf waves are forced by the local winds. The low-frequency current oscillations due to the shelf waves can cause sediment resuspension and contribute to cross-shelf transport of fine sediment. Further analyses of these possible shelf waves are not presented here.

Coherences were computed between the currents over their full depth range and east–west (EW) and north–south (NS) wind stresses (not shown). The V current components were marginally coherent with the wind stress. The U current components, however, were influenced by the winds over the bank. The winds highly impacted (multiple coherences up to 66%) currents in the upper 20 m near frequencies associated with periods of a week to ten days, which is suggestive of some wind effects on the surface currents associated with frontal passages. Results from coherence analyses also show that the EW current fluctuations at these periods of about a week to ten days were significantly coherent with the NS wind stress but not so with the EW wind stress, suggesting that the current fluctuations are influenced by the cross-shelf wind-stress component. These results may seem contrary to results presented by Cochrane and Kelly (1986). They suggest that the currents in general west of 92.5°W are influenced primarily by the alongshore component of the wind stress but are more weakly influenced east of 92.5°W. However, their coherency spectra also shows that the cross-shelf wind stress is significant with both the alongshore and cross-shelf currents at periods of about ten days in agreement with our results.

To investigate large-scale features of the currents and to explore the extent to which the velocities at different depths are correlated an empirical orthogonal function (EOF) analysis was conducted. The larger scale correlated modes of motion over and around the bank are extracted in order to provide a simpler picture of the dominant current variability. At each ADCP location an EOF analysis was done on U(z,t) and V(z,t) (functions of depth (z) and time (t)). To compute EOFs for both velocity components simultaneously, U and V were further concatenated to form a single array (at each ADCP location): UV=[U(z,t),V(z,t)], which was then analyzed as a scalar array. This method is described by Preisendorfer (1988) and Kaihatu et al. (1998). The method yields a set of eigenfunctions (EOFs; functions of z, mode) and principal components (PCs; functions of t, mode). The resulting eigenfunctions were separated into U and V parts and speed and orientation profiles formed for each mode; as with principal ellipses, an orientation of θ is equivalent to θ+180°. The eigenfunctions were dimensionalized by multiplication by the square root of the eigenvalue. These then yield magnitudes and orientations of the fluctuations associated with each mode. Modes 1 and 2 accounted for at least 70% of total variance; M5 was significantly higher since the data were limited to the upper ~50 m, where depth

dependence was minimal. Mode 1 accounted for at least 53% of all variance and was clearly dominant compared to Mode 2, whose maximum was about 20%.

Shallower than about 50 m, Mode 1 magnitudes were at their largest and indicated that velocities in this depth interval were vertically correlated (the M5 profiles fell off above 50 m, due to the proximity of the bottom), and may indicate a frictional (Ekman) layer. Orientations above 50 m were ~E–W, as for the principal ellipses. Below 50 m, profile magnitudes for M2 and M4 fell off more rapidly than for M1 and M3, indicating lower vertical correlations with shallower depths for M2 and M4; this difference was likely due to the greater rotation with depth, from E–W, required for deep velocities to be aligned with the constraint of local bathymetry at these locations. The orientation profile for M1, rotated slightly with depth to about WSW–ENE; for M3, it rotated further to about SW–NE. At all locations, Mode 1 PCs were highly correlated (at least 0.97) with the depth-averaged eastward (U) velocity. A second EOF analysis was done using velocity anomalies about vertical averages at each location, to better isolate baroclinic variability. The results were not quite as robust (explained variances for Mode 1 are about 40–45%). The Mode 1 eigenfunction magnitude profiles for M1–M4 nearly overlay each other and ranged from maxima of about 5 cm/s near surface and bottom, with zero crossings near 55 m; for M5, the profile was similar, but shallower. Orientations profiles for this case were also mainly E–W. Correlation coefficients between Mode 1 PC series for M1–M4 showed agreement, which was due mainly to the shallower E–W variability. The lowest value (0.63) was for M3 and M2, located near the southern edge of the bank. The largest value (0.91) was for M1 and M4, located north and east of the bank, respectively.

6. Temperature and salinity

Temperature sections, smoothed over 6 h, are shown in Fig. 15. The vertical striping near the diurnal tidal frequency throughout the records could have been enhanced by the inertial oscillations. Salinity measurements were quite noisy and high-resolution salinity sections are not shown. String sensors were subject to heavy biofouling noted during their recovery. Conductivity measurements were most affected and there were numerous spikes and drifts in the calculated salinity. However, low-resolution salinity time series are shown in Fig. 16(b). Here the salinity was filtered with a median filter that was 1-day long and then a single point was plotted for each day. The median filter effectively eliminated borderline wild points and should provide a more realistic salinity. The temperature time series were correspondingly filtered for comparison with the salinity time series and are shown in Fig. 16(a). There was little stratification in the water column from the beginning of the deployment to about day 90 (March 31). Temperature range over the water column was only

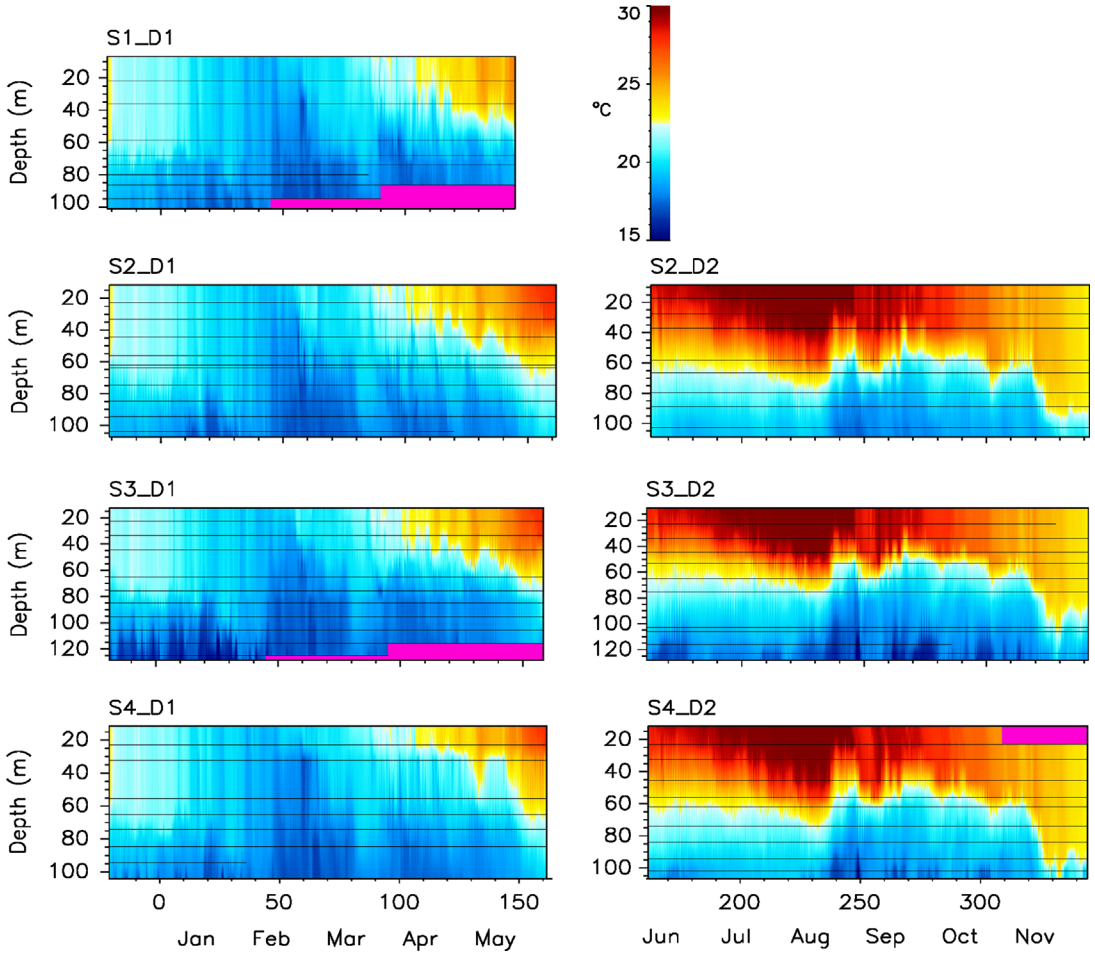

Fig. 15. Temperature time series are shown for the four string moorings (S1–S4). Note that S2 was not redeployed for the summer–fall period. The pink color indicates no data. Horizontal lines indicate vertical positions of the sensors, using the average pressures. Truncated lines indicate bad or missing data, which have been vertically interpolated. The *x*-axis shows days and months relative to 2011. (For interpretation of the references to color in this figure legend, the reader is referred to the web version of this article.)

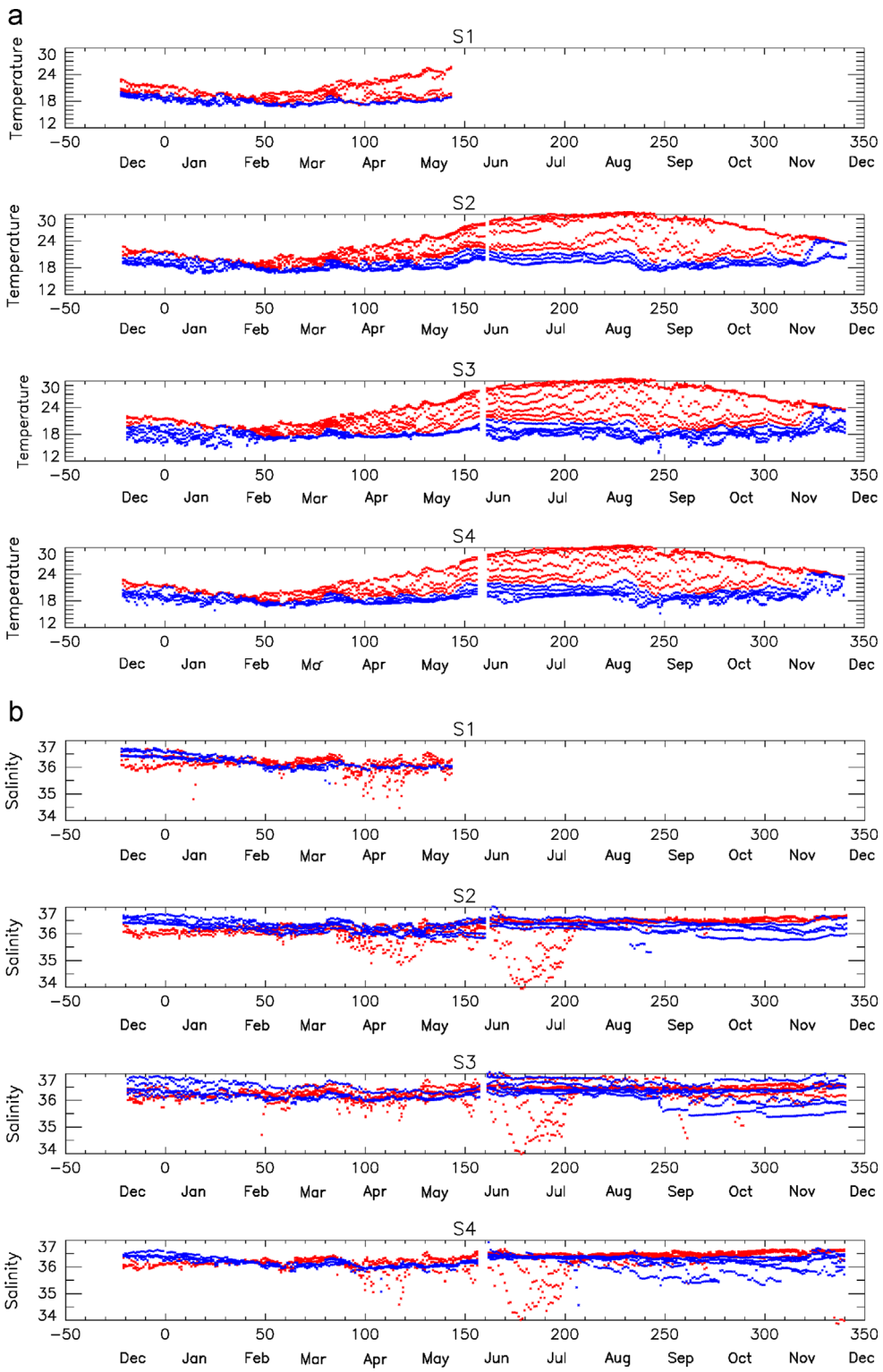

Fig. 16. (a) Temperature time series for the four string moorings at 1-day resolution. (b) Corresponding salinity time series. Above 75–80 m (red), and below 75–80 m (blue). The *x*-axis shows days and months relative to 2011. (For interpretation of the references to color in this figure legend, the reader is referred to the web version of this article.)

about 3 °C while the salinity range was generally less than 1 psu and sometimes much less (S4, day 40, about 0.2 psu). Stratification gradually increased from day 90 to day 250 (March 31 to September 7) where temperature ranged about 12 °C over the water column, and then decreased back to the range observed during beginning of the deployment (in December 2010 and 2011). Drifts in salinity may have occurred for some of the instruments after day 200 (July 19). However, similar patterns of decreasing salinity occurred at each of the string moorings, suggesting that at least the trend of decreasing salinity may be real. In addition, the decreasing salinity trend appeared mostly in the lower water column where biofouling was not as much of an issue as in the upper water column.

Temperature over the entire year ranged from about 16° to 30 °C while salinity ranged from about 34 psu to almost 37 psu. Salinity values were typically greater than 36 psu, reflective of

salinities off the shelf and south of the bank. The observed annual temperature range agrees with historical data, e.g., Lugo-Fernández (1998); but the salinity range observed is smaller than at other times; see Deslarzes and Lugo-Fernández (2007) and references therein. However, salinities within a few meters of the surface were not measured. Historically, the low salinity events tend to have salinities of 30–33 psu that occur near summer maxima in surface temperature but associated with a temperature drop (Deslarzes and Lugo-Fernández, 2007).

Two periods in which salinities were significantly lower than usual in the upper water column occurred approximately between days 90 and 120 (March 31 and April 30) and days 150 and 200 (May 30 and July 19). During the first event, the salinities decreased to about 35 psu and during the second event they decreased to about 34 psu. The two low salinity events were associated with warmer water in the top part of the water column (Fig. 15). The generation mechanism for this type of event could possibly be entrainment of shelf water by an eddy at the shelf edge. In addition, a relatively low temperature range of about 2 °C throughout the water column was observed between days 40 and 60 (February 9 and March 1) (Figs. 15 and 16a). The salinity time series (Fig. 16b) shows a few salinities lower that 36 ppt during this time period. The cooler and less saline water was likely transported by southwestward currents (Fig. 8) over the bank by eddy activity since the winds were mostly out of the south (Fig. 2).

Bottom temperatures acquired from the ADCPs in the Barny moorings are shown in Fig. 17. Similar patterns in temperature fluctuations were found between the moorings. Records for M1–M4 show similar low-frequency variations; of these, the largest differences were exhibited by M3, which was deployed closer to the shelf break and 25–30 m deeper than the other three. The record from M5 was from shallower than 50 m and shows an overall higher temperature and more variability than the deeper records. Interestingly, a sudden temperature drop of about 6 °C (29 °C to 23 °C) occurred over two days (days 236–238) at M5 located on top of the bank. Drops of 2–3 °C also occurred at about the same time at each of the other moorings. A second drop in temperature closely followed. Temperatures at M5 fell to 22 °C at day 246 and near the same time fell 3–4 °C at M3 and M4, with low temperatures of 14 °C and 15 °C recorded at M3 and M4, respectively. Temperature at M2 fell less than a degree. At approximately day 250, the temperature at M5 increased by about 7 °C (21–28 °C) over a period of about four days (days 246–250) which is also evident to a lesser degree at each of the other moorings. A similar, but less extreme, temperature fluctuation began at day 260.

These drops in temperature were evident in the temperature sections (Fig. 15) over most of the water column. From the temperature section for S3-D2 (Fig. 15), colder water from approximately 75 m depth rose 30 m to about 45 m depth (days 236–238). The temperature time series (Fig. 16a) also showed these drops in temperatures at each of the string moorings. In particular, significant drops in temperature occurred at S3 and S4 where anomalous temperatures of 14 °C and 15 °C, respectively, were also observed near the bottom. Corresponding drops in salinity to about 35.5 psu (Fig. 16b) were found in conjunction with the temperature drops.

There is evidence that the temperature and salinity drops were wind related. At M3, between depths of about 60 m and the bottom, relatively strong southwestward currents (Fig. 8) were observed for several days around day 250, aligned with the topography of the bank. These currents may have been in response to a storm event that lasted about a week and winds peaked at about 27 kts (14 m/s; Fig. 2 near day 250). Hence, less saline shelf water over the EFGB was likely driven from the inner shelf by winds. Movement of low salinity pools of water off the inner shelf by strong north winds have been described in detail and referred to as “squirts” by Walker et al. (1996). The cooler waters observed here near the bottom at the EFGB must have originated in deeper water off the shelf and were likely due to upwelling or vigorous mixing induced by the strong event of southwestward winds that rotated to southeastward during the event. Climatological temperature profiles (Boyer et al., 2009), and temperature sections just south of the EFGB by McGrail and Carnes (1983) and Nowlin and Parker (1974) show that the 14 °C waters are typically found at 200 m water depth. Therefore, water at depths of at least 200 m can be mixed into the upper water column and hence affect the upper portions of the EFGB.

For calculation of mixed-layer depth (MLD), the temperature profiles from the string moorings, each consisting of about ten observations over the water column, were interpolated to 1-meter intervals. Temperatures were not extrapolated to the surface. The MLD was then set at the depth level where the temperature changed by at least 0.25 °C from the shallowest temperature measurement. Upon visual inspection of typical individual temperature profiles, this criterion provided reasonable MLDs over the entire data set. To reduce the higher frequency variability, the MLDs were smoothed over about a day. The average MLD over all the strings was also computed and a 5-day boxcar average was applied to reduce the daily variability. The MLDs are shown in Fig. 18 for each of the string moorings, along with their composite 5-day average. MLDs ranged from about 60 to 80 m from mid-

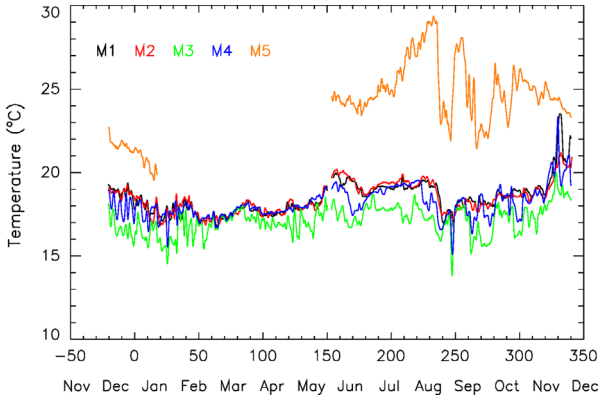

Fig. 17. Bottom temperatures from the ADCP moorings (M1–M5). The *x*-axis shows days and months relative to 2011.

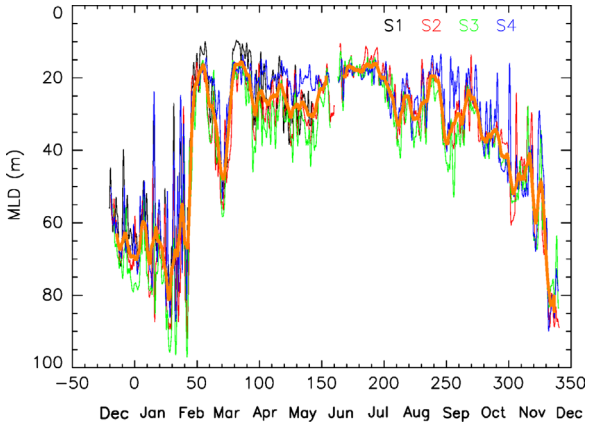

Fig. 18. Mixed-layer depths computed from the string mooring temperature observations. Mixed-layer depths for each string (denoted by the color key in the upper right corner) were smoothed over a day. The orange curve is the 5-day average of the mixed-layer depths for the individual strings. The *x*-axis shows days and months relative to 2011. (For interpretation of the references to color in this figure legend, the reader is referred to the web version of this article.)

December 2010 until February 2011 and then MLDs rapidly decreased to less than 20 m over a period of about 2 days. This large change in MLD was associated with the cyclonic eddy discussed in Section 5. The MLD increased to over 50 m as the eddy moved out and decreased to 20 to 40 m until mid-October where it gradually increased to 60–80 m toward the end of the deployment period in December 2011. The mixed layer was deepest during the months of December and January) and ranged from about 60–80 m in depth. MLDs ranged between 20 and 40 m for much of the year (March–October). November appeared to be a transition month (at least for 2011) where the MLD increased to depths greater than 60 m. Fluctuations in the MLD of 10–20 m at periods of about a week were likely related to atmospheric frontal passages. This seasonal cycle of the mixed layer at the FGB is similar to that reported by McGrail (1983). Deepening of the MLD occurred from December to February and then rapidly decreased. This trend in MLD during this time period may be related to reduced solar heating and increased wind mixing and has been observed in the data from Kara et al. (2003) and Monterey and Levitus (1997).

7. Summary

The EFGB interrupted the along shelf current flow and resulted in a two-layer current system in the vicinity of the bank. Currents at the EFGB were generally eastward throughout the year in the upper part of the water column above the sill of the bank but were reversed for periods from a day to a week or more by cyclonic eddies impinging on the edge of the shelf. These cyclonic eddies may have originated as LC frontal eddies that were transferred to warm core rings upon separation. The currents were reversed to westward flow in the upper water column from a few days to several weeks during March (days 60–80), October (days 270–300), and November (days 310–330). The bank impacted the flow in the lower water column and the flow followed the bathymetry. Near-bottom currents at the southwestern (M2) and southeastern (M3) corners of the bank were mostly directed offshore throughout the year in southeastward and southwestward directions, respectively, following the bathymetry. Average southward or offshore currents in the lower layer of the water column were sometimes comparable or larger than the east–west currents in the upper water column. The maximum observed offshore (onshore) velocity was 27 cm/s (20 cm/s). The region just south of the EFGB could be an area of convergence for the deep offshore flow. Integral time scales for the cross-shelf flows generally ranged from 3 to 5 days throughout the water column while the time scales for the along-shelf flows were longer and ranged from about a week to more than 2 weeks.

The main tidal components were M2, K1, and O1 but tidal currents were weak at the EFGB. However, inertial currents (periods near the O1 tide) were often significant and could reverse the generally eastward low-frequency surface flows for a few hours when these background currents were weak. The inertial currents are enhanced during summer when in phase with wind modulations due to sea-breeze effects and can easily exceed 20 cm/s. Since the radius of the bank is only about 4 km, a 10 cm/s current can move matter from the top of the bank to off the bank in about half a day. Nevertheless, these westward-induced short-term currents are not persistent enough for direct westward advection of particle off the bank to other banks.

Some correlations with the winds were found. However, the generally eastward current flow over the EFGB was not correlated with EW wind stress but likely is the southern limb and return flow of the cyclonic gyre on the Louisiana–Texas shelf that is driven by westward winds on its northern limb (Cochrane and Kelly, 1986). A significant southward component of the flow through much of the water column was caused by a storm event in September. During this event, the correlation of the southward flowing currents with winds blowing from the north was high and lower salinity shelf waters were driven from the inner shelf to over the EFGB. Interestingly, EW current fluctuations at periods of about a week to ten days were significantly coherent with the NS wind stress (cross-shelf wind-stress component) but not so with the EW wind stress.

Mixed layers often extended to the bottom on top of the bank and ranged from as shallow as 10 m to deeper than 80 m just off the bank. Mixed-layer depths changed rapidly and were observed to shallow from about 80–20 m in less than 2 days due to an eddy passage that transported cooler shelf water over the bank. Mixed layers were deepest (60–80 m) during December and January and generally ranged between 20 and 40 m for much of the year. November was the transition month for the seasonal deepening of the mixed layer.

The southward deep flows at the southern edge of the EFGB in conjunction with the well-known westward motion of LC warm core eddies, and associated cyclonic and anticyclonic eddies, may be a major conduit for shelf water exchange between the Flower Gardens and rest of the Gulf. Conversely, the less-frequent northward deep flows at the southern edge of the bank can transport deep ocean water onto the shelf and Flower Gardens. Offshore flows at the EFGB were largest in the October to December time period for 2011. Much of the cross-shelf exchange is likely to occur in the lower-water column and near the bottom. Eddies do not necessarily have to pass directly over the bank to transfer particulates that reside on the bank since they can entrain the offshore flow. Upwelling in response to storms can also transport cooler deeper waters onto the shelf. One such event was observed during a high wind period during September where 14 °C water was upwelled from depths exceeding 200 m onto the shelf. In addition, shelf waves may contribute to the shoreward and offshore flows near the bottom. Numerous other banks in the Flower Garden Sanctuary can then be affected, as well as other regions in the Gulf of Mexico and in the Atlantic Ocean through eddies and the LC connectivity as shown herein and by Lugo-Fernández et al. (2001) and Lugo-Fernández (2006). Similar processes should also be common at the WFGB, similarly located at the shelf edge. Upper layer currents generally did not reverse towards the west for long enough periods to connect the EFGB with the WFGB. However, connections between the EFGB to the WFGB can be made through the train of westward propagating eddies, as discussed by Lugo-Fernández et al. (2001) using surface drifters. The WFGB can also connect with the EFGB through the generally eastward upper-layer flows. Connectivity between the banks is expected to be higher during LC ring passages.

Acknowledgments

This work was sponsored by the Bureau of Ocean Energy Management (BOEM; formerly Minerals Management Service) in the project referred to as the “Currents Over Banks (COB)” through Interagency Agreement no. M10PG00038 and by the Office of Naval Research in a Naval Research Laboratory (NRL) project referred to as “Mixing Over Rough Topography (MORT)”. The measurements were made in cooperation with the Flower Garden Banks National Marine Sanctuary (administered by the National Oceanic and Atmospheric Administration (NOAA)). Thanks are extended to our mooring team of Mark Hulbert, Andrew Quaid, and Justin Brodersen of NRL, and to Steve Sova of QinetiQ.

References

Beard, D.W., 1984. Wind-induced circulation on the outer continental shelf of Texas, Spring 1982. M.S. Thesis, Department of Oceanography, Texas A&M University, College Station, Texas. 128.

Boyer, T.P., Antonov, J.I., Baranova, O.K., Garcia, H.E., Johnson, D.R., Locarnini, R.A., Mishonov, A.V., O'Brien, T.D., Seidov, D., Smolyar, I.V., Zweng, M.M., 2009. World Ocean Database 2009. In: Levitus, S. (Ed.), NOAA Atlas NESDIS 66. US Government Printing Office, Wash., D.C., pp. 206.

Brooks, D.A., 1983. The wake of Hurricane Allen in the western Gulf of Mexico. Journal of Physical Oceanography 13, 117–129.

Blaha, J., Sturges, W., 1981. Evidence for wind-forced circulation in the Gulf of Mexico. Journal of Marine Research 39 (4), 711–734.

Carnes, M.R., Teague, W.J., Jarosz, E., 2008. Low-frequency current variability observed at the shelfbreak in the northeastern Gulf of Mexico: November 2004–May 2005. Continental Shelf Research 28 (3), 399–423, http://dx.doi.org/10.1016/j.csr.2007.10.005.

Chen, C., Reid, R.O., Nowlin Jr., W.D., 1996. Near-inertial oscillations over the Texas–Louisiana shelf. Journal of Geophysical Research 101, 3509–3524.

Cho, K., Reid, R.O., Nowlin Jr., W.D., 1998. Objectively mapped steam function fields on the Texas–Louisiana shelf based on 32 months of moored current meter data. Journal of Geophysical Research 103 (C5), 10,377–10,390.

Cochrane, J.D., Kelly, F.J., 1986. Low-frequency circulation on the Texas–Louisiana continental shelf. Journal of Geophysical Research 91, 10645–10659.

Cutchin, D.L., Smith, R.L., 1973. Continental shelf waves: low-frequency variation in sea level and currents over the Oregon continental shelf. Journal of Physical Oceanography 3, 73–82.

Daddido, E., Wiseman, W.J., Murray, S.P., 1978. Inertial currents over the inner shelf near 30 N. Journal of Physical Oceanography 8, 728–733.

Deslarzes, K.J.P., Lugo-Fernández, A., 2007. Influence of terrigenous runoff on offshore coral reefs: an example from the Flower Garden Banks, Gulf of Mexico. In: Aronson, R.B. (Ed.), Geological Approaches to Coral Reef Ecology: Placing the Current Crises in Historical Context. Springer Verlag, pp. 126–160.

DiMarco, S.F., Reid, R.O., 1998. Characterization of the principal tidal current constituents on the Texas–Louisiana shelf. Journal of Geophysical Research 103, 3093–3109.

Dodge, R.E., Lang, J.C., 1983. Environmental correlates of hermatypic coral (*Montastrea annularis*) growth on the East Flower Gardens Bank, northwest Gulf of Mexico. Limnology and Oceanography 28, 228–240.

Gill, A.E., Schumann, E.H., 1974. The generation of long shelf waves by the wind. Journal of Physical Oceanography 4, 83–90.

Gittings, S.R., 1998. Reef community stability on the Flower Garden Banks, northwest Gulf of Mexico. Gulf of Mexico Science 16, 161–169.

Gutierrez de Velasco, G., Winant, C.D., 1996. Seasonal patterns of wind stress and wind stress curl over the Gulf of Mexico. Journal of Geophysical Research 101 (18), 127–18140.

Halper, F.B., McGrail, D.W., Merrell Jr., W.J., 1988. Seasonal variability in the currents on the outer Texas–Louisiana shelf. Estuarine, Coastal and Shelf Science 26, 33–50.

Hamilton, P., 1992. Lower continental slope cyclonic eddies in the central Gulf of Mexico. Journal of Geophysical Research 97, 2185–2200.

Hamilton, P., Berger, T.J., Johnson, W., 2002. On the structure and motions of cyclones in the northern Gulf of Mexico. Journal of Geophysical Research 107 (C12) (Article no. 3208).

Jarosz, E., Murray, S.P., 2005. Velocity and Transport Characteristics of the Louisiana–Texas Coastal Current. Circulation in the Gulf of Mexico: Observations and Models, Geophysical Monograph Series 161. American Geophysical Union, http://dx.doi.org/10.1029/161GM11.

Jarosz, E., Hallock, Z.R., Teague, W.J., 2007. Near-inertial currents in the DeSoto Canyon region. Continental Shelf Research 27, 2407–2426.

Kaihatu, J.M., Handler, R.A., Marmorino, G.O., Shay, L.K., 1998. Empirical orthogonal function analysis of ocean surface currents using complex and real-vector methods. Journal of Atmospheric and Oceanic Technology 15, 927–941.

Kara, A.B., Rochford, P.A., Hurlburt, H.E., 2003. Mixed layer depth variability over the global ocean. Journal of Geophysical Research 108, 3079, http://dx.doi.org/10.1029/2000JC000736.

Ko, D.S., Martin, P.J., Rowley, C.D., Preller, R.H., 2008. A real-time coastal ocean prediction experiment for MREA04. Journal of Marine Systems 69 (1-2), 17–28 http://dx.doi.org/10.1016/j.jmarsys.2007.02.022.

Kubota, M., Nakata, K., Nakamura, Y., 1981. Continental shelf waves off the Fukushima Coast Part I: observations. Journal of the Oceanographical Society of Japan 37, 267–278.

Lugo-Fernández, A., 1998. Ecological implications of hydrography and circulation to the Flower Garden Banks, northwest Gulf of Mexico. Gulf of Mexico Science 16, 144–160.

Lugo-Fernández, A., 2006. Travel times of passive drifters from the western Caribbean to the Gulf of Mexico and Florida–Bahamas. Gulf of Mexico Science 24, 61–67.

Lugo-Fernández, A., Deslarzes, K.J.P., Price, J.M., Boland, G.S., Morin, M.V., 2001. Inferring probable dispersal of Flower Garden Banks coral larvae (Gulf of Mexico) using observed and simulated drifter trajectories. Continental Shelf Research 21, 47–67.

McGrail, D.W., Carnes, M., 1983. Shelfedge dynamics and the nepheloid layer in the northwestern Gulf of Mexico. SEPM Special Publication 33, 251–264.

McGrail, D.W., 1983. Flow, boundary layers, and suspended sediment at the Flower Garden Banks. In: Rezak, R., Bright, T.J, McGrail, D.W. (Eds.). Reefs and banks of the northwestern Gulf of Mexico: their geological, biological, and physical dynamics. Final Report, Technical Report no. 83-1-T., U.S. Department of the Interior, Minerals Management Service, Gulf of Mexico OCS Regional Office, New Orleans, LA. pp 141–230.

Monterey, G., Levitus, S., 1997. Seasonal Variability of Mixed Layer Depth for the World Ocean, NOAA Atlas NESDIS 14. US Government Printing Office, Washington, DC p. 100.

Moum, J.N., Nash, J.D., 2000. Topographically induced drag and mixing at a small bank on the continental shelf. Journal of Physical Oceanography 30, 2049–2054.

Moum, J.N., Nash, J.D., 2008. Seafloor pressure measurements of nonlinear internal waves. Journal of Physical Oceanography 38, 481–491.

Mooers, C.N.K., Smith, R.L., 1968. Continental shelf waves off Oregon. Journal of Geophysical Research 73, 549–557.

Nowlin Jr., W.D., Parker, C.A., 1974. Effects of a cold-air outbreak on shelf waters of the Gulf of Mexico. Journal of Physical Oceanography 4, 467–486.

Nowlin, W.D., Jr., Jochens, A.E., Reid, R.O., DiMarco, S.F., 1998. Texas–Louisiana Shelf Circulation and Transport Process Study: Synthesis Report, LATEX A. OCS Study MMS 98-0035 and MMS 98-0036, vols. I and II, US Department of the Interior, Minerals Management Service, Gulf of Mexico OCS Region, New Orleans, Louisiana.

Nowlin Jr., W.D., Jochens, A.E., DiMarco, S.F., Reid, R.O., Howard, M.K., 2005. Low-frequency circulation over the Texas–Louisiana continental shelf. Circulation in the Gulf of Mexico: observations and models, Geophysical Monograph Series 161. American Geophysical Union, http://dx.doi.org/10.1029/161GM17.

Oey, L.-Y., 1995. Eddy and wind-forced shelf circulation. Journal of Geophysical Research 100, 8621–8637.

Perkins, H., De Strobel, F., Gauldesi, L., 2000. The barny sentinel trawl-resistant ADCP bottom mount: design, testing, and application. IEEE Journal of Oceanic Engineering 25, 430–436.

Price, J.F., 1976. Several aspects of the response of shelf waters to a cold front passage. Memoires Societe des Sciences de Liege, 6e Series X, 201–208.

Preisendorfer, R.W., 1988. Principal Component Analysis in Meteorology and Oceanography. Elsevier p. 425.

Rezak, R., Gittings, S.R., Bright, T.J., 1990. Biotic assemblages and ecological controls on reefs and banks of the northwest Gulf of Mexico. American Zoologist 30, 23–35.

Sahl, L.E., 1984. Suspended sediment on the upper Texas continental shelf. Ph.D. Dissertation. Department of Oceanography, Texas A&M University, College Station, Texas. 184.

Sturges, W., Blaha, J.P., 1976. A western boundary current in the Gulf of Mexico. Science 192, 367–369.

Teague, W.J., Jarosz, E., Carnes, M.R., Mitchell, D.A., Hogan, P.J., 2006. Low-frequency current variability observed at the shelfbreak in the northeastern Gulf of Mexico: May–October 2004. Continental Shelf Research 26, 2559–2582.

Walker, N.D., Huh, O.K., Rouse Jr., L.J., Murray, S.P., 1996. Evolution and structure of a coastal squirt off the Mississippi River delta: Northern Gulf of Mexico. Journal of Geophysical Research, 101; pp. 20,643–20,655.

Walker, N.D., Hammack, A.B., 2000. Impacts of winter storms oncirculation and sediment transport: Atchafalaya–Vermillion Bay Region, Louisiana, U.S.A.. Journal of Coastal Research, 16; pp. 996–1010.

Wolanski, E., Burrage, D., King, B., 1989. Trapping and dispersion of coral eggs around Bowden Reef, Great Barrier Reef, following mass coral spawning. Continental Shelf Research 9, 479–496.

Zhang, X., DiMarco, S.F., Smith IV, D.C., Howard, M.K., Jochens, A.E., Hetland, R.D., 2009. Near-resonant ocean response to sea breeze on a stratified continental shelf. Journal of Physical Oceanography 39, 2137–2155.